Volcanoes at Divergent Plate Boundaries

11

11.1 Introduction

This chapter focuses on divergent plate boundaries, that is where two lithospheric plates drift away from each other. Plate divergence may occur on continental, transitional and oceanic lithosphere, with spreading rates varying over nearly 2 orders of magnitude, from a few mm/year to ~15 cm/year. Except for the continental and oceanic boundaries characterized by the lowest bound of spreading rates, divergent plate boundaries are commonly associated with widespread magmatic activity. For decades it has been assumed that such a magmatic activity is a mere product of the regional tectonic processes responsible for plate divergence. Recent geological, geophysical and geodetic data have highlighted a much more active role of magma in separating the plates, independently of the nature of the rifted crust, allowing redefining the tectono-magmatic relationships of divergent plate boundaries.

This chapter follows the steps of the Wilson cycle for divergent plate boundaries describing the progression from slowly spreading immature continental rifts to fast spreading oceanic ridges. The main aims of this chapter are to:

- describe the tectono-magmatic features of representative cases of divergent plate boundaries;
- highlight similarities and differences in the magmatic activity as a function of the spreading rate on continental, transitional and oceanic crust;
- propose a general model summarizing the role of magmatic activity in the evolution of divergent plate boundaries.

11.2 Continental Rifts: The East African Rift System

Several rift zones can be found on the continents. As described in Chap. 2, those associated with magma are usually narrow rifts, such as the Rio Grande Rift (southern USA), the Rhine Graben (western Europe), the Baikal Rift (central Asia) and the East African Rift System. Of these, only the latter is a magmatic continental rift along a divergent plate boundary: therefore, this section focuses on its tectonic and magmatic features.

The East African Rift System (EARS) separates the Nubian plate from the Somali plate, stretching over nearly 5000 km onland, from Mozambique to the triple junction of Afar (Ethiopia), where the EARS meets the Gulf of Aden and Red Sea oceanic rifts (Fig. 11.1). Despite its overall structural continuity, the EARS is not homogeneous, consisting of several

V. Acocella, *Volcano-Tectonic Processes*, Advances in Volcanology,
https://doi.org/10.1007/978-3-030-65968-4_11

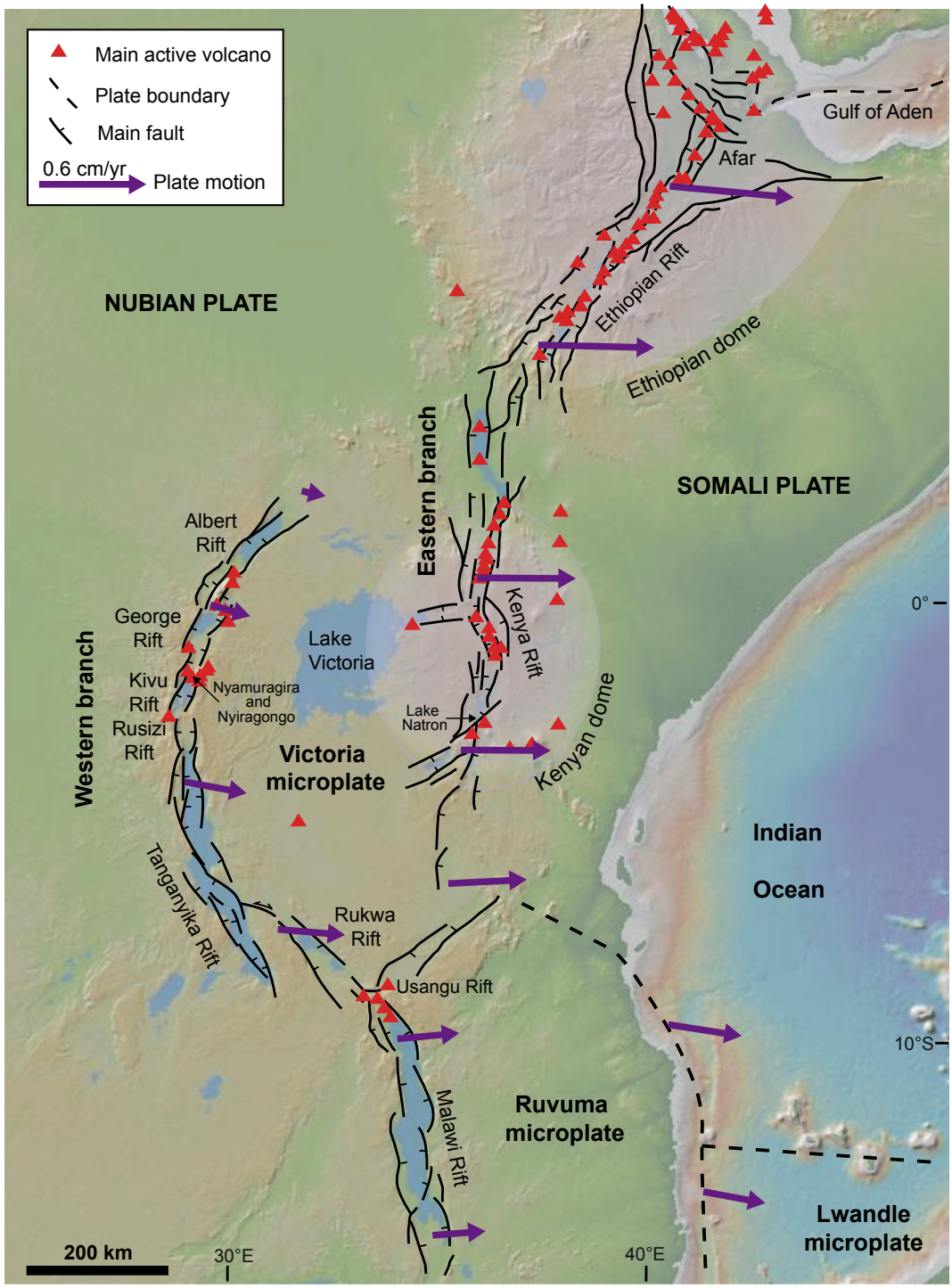

Fig. 11.1 Main volcano-tectonic features of the East African Rift System. Plate velocity vectors (with respect to a fixed Nubian plate; from Stamps et al. 2018, and references therein). Base DEM provided by GeoMapApp

branches forming three microplates: Victoria, Ruvuma and Lwandle. There is an overall northward increase in the ~E–W trending amount of extension, passing from 0.2 to 0.3 cm/year to the south to ~0.7 cm/year to the north, before reaching Afar. This corresponds to an overall northward decrease in the crustal thickness, an increase in the magmatism and volcanic activity and the shallowing of earthquakes. In particular, the southern predominantly amagmatic portion shows seismicity down to 30–40 km of depth, suggesting rift border faults are active at lower crustal levels, whereas the northern predominantly magmatic portion of the EARS shows seismicity mostly shallower than 15 km (Keir et al. 2006; Craig et al. 2011; Perez-Gussinye et al. 2009; Ebinger et al. 2017; Stamps et al. 2018). These features highlight an interdependence among the amount of extension, the resulting crustal thinning and decompression melting, and magma generation and volcanic activity, ultimately also thinning the seismogenic crust. In addition, the ages of the erupted products indicate an overall southward migration of volcanic activity, from Ethiopia to Tanzania, suggesting that the most extended northern rift portion is also older. This tectonic and volcanic gradient along the EARS may result from several processes, including plumes and superplumes initiating rifting, as below the Ethiopian and Kenyan portions, and the reactivation of pre-existing mobile belts (Ebinger and Sleep 1998; Corti et al. 2007; O'Connor et al. 2019; Rooney 2020a).

The southernmost portion of the EARS consists of the onshore western system (the Malawi Rift) and the offshore eastern system (the Mozambique Basin) and lacks volcanism (Fig. 11.1). The Malawi Rift has an overall asymmetric structure, with interacting half-grabens with alternating polarity, each forming a ~100 km long and ~50 km wide basin. Pronounced heat flow focuses in regions of asthenospheric upwelling and in ancient magmatic rift segments. The offshore eastern system enters the oceanic lithosphere, with an overall amount of extension between 5 (to the south) and 12 (to the north) kilometres and sporadic magmatic intrusions (Ebinger et al. 1984; Franke et al. 2015; Deville et al. 2018; Njinju et al. 2019).

North of the Malawi Rift, the EARS branches into an eastern and western portion, both initiated at ~25 Ma (Fig. 11.1). The connection with the offset western branch occurs through the highly oblique Rukwa Rift, with localized volcanism. Along the northwest continuation of the Rukwa Rift, the western branch of the EARS bends to a N–S direction, reflecting the perturbation of the tensional stress field along the west side of the stronger Tanzanian craton (Ebinger et al. 1989; Corti et al. 2007). The western branch of EARS is 40–70 km wide and has experienced crustal extension of less than 15%, with widespread seismicity and asymmetric structure, consisting of interacting half-grabens. Volcanism has been mainly occurring in the last 11 Ma between the half-grabens, as in the Nyiragongo dome, hosting the Nyamuragira and Nyiragongo volcanoes (Ebinger 1989a, b; Upcott et al. 1996; Wadge et al. 2016).

The eastern branch of the EARS is magmatically more active and consists of two main portions, centred on the Kenyan and Ethiopian domes (Fig. 11.1; e.g., Rooney 2020a, b and references therein). Both domes are uplifted crust resulting from the thermal buoyancy of mantle plumes below. The Kenyan dome, which uplifted to more than 1400 m by at least 13.5 Ma, lies on a long-lived low seismic velocity zone, extending to ~150 km depth, possibly feeding mafic underplating in the lowermost crust. Above, a ~N–S trending asymmetric rift consisting of interacting half-grabens reactivates pre-existing structures. The rift thins the ~40 km thick crust to ~35 (to the south) and ~20 km (to the north), with extension varying from 5–10 to 35–40 km, respectively (Dugda et al. 2005; Park and Nyblade 2006). Many Kenyan volcanoes have ~NW–SE elongated summit calderas parallel to the direction of the minimum principal stress σ_3, suggesting a far-field control on the elongation of the magma chambers below (Bosworth et al. 2003). The Kenya Rift shows a more advanced stage of tectonic and magmatic activity with regard to the western branch, at the same latitude. This activity also manifests through

unrest and eruptions at several volcanoes and through rifting events involving seismicity along regional normal faults and dike injections, as observed at Lake Natron in 2007. During this event, the opening of the rift was achieved through two contemporaneous processes. One was regional normal faulting, responsible for a nearly 3 months long seismic swarm with the seismic moment much higher than the geodetic moment, and culminating in its early phase with a magnitude *M5.9* earthquake. This seismicity may have been induced by a pressurized deep magma chamber. The other was the emplacement of a ~1.5 m thick dike between 2 and 6 km of depth, which followed the peak in seismicity and was responsible for most of the measured rift opening (Calais et al. 2008; Reiss et al. 2021 and references therein).

To the north of the Kenyan dome is the Ethiopian dome, which includes the continental Main Ethiopian Rift, described in Sect. 11.2.1, and the transitional Afar triple junction, described in Sect. 11.3.

11.2.1 The Main Ethiopian Rift

The continental Main Ethiopian Rift (MER) and the adjacent transitional crust of Afar are the ideal sites to study the tectono-magmatic features of a nascent divergent plate boundary. Indeed, within a thousand of kilometres, incipient continental rifting (southern MER) evolves into mature continental rifting (northern MER) and continental break-up (central Afar) to proto-oceanic rifting (northern Afar; Fig. 11.2). These variations allow investigating and comparing contiguous rift portions at progressively more advanced evolutionary stages, providing important insights on the early phases of plate divergence.

The MER-Afar system lies on the Ethiopian dome, resulting from a broad uplift due to the activity of the Afar mantle plume, presently identified as a more than 400 km deep and more than 500 km wide low-wave speed anomaly beneath Afar and the MER (Mohr and Wood 1976; Ebinger and Sleep 1998; Benoit et al. 2006). Shallow tomographic data allow capturing the current structure of the MER-Afar area at a depth of several tens of kilometres, suggesting pervasive partial melt, with focused upwelling and melt storage beneath the MER, where the slowest velocities are observed. Average crustal shear velocity is faster beneath Afar than the MER, albeit Afar has localized slow velocities beneath active volcanic centres. These slow-velocity regions in the MER-Afar systems are interpreted as due to magmatic intrusions and crustal heating (Chambers et al. 2019).

As observed along the EARS, in the MER-Afar system there is also a progressive northward increase in extension rate and a parallel decrease in lithospheric thickness: as a result, the frequency of volcanoes also increases northward. The NE-SW trending MER developed in two main stages under predominant oblique opening, with an overall ~E–W direction of divergence. Mio-Pliocene continental rifting first activated the NE–SW striking border faults, creating up to 5 km of subsidence, and was accompanied by diffuse magmatic activity, also off-rift. During the Quaternary, tectonic and magmatic activity focused in NNE-SSW trending narrow zones within the rift, deactivating the border faults (Fig. 11.2; Mohr 1967; Corti 2009). The two evolutionary stages can be also recognized along different portions of the current MER. The less-extended southern MER has a ~40 km thick crust and is in incipient continental rifting, with most of the deformation accommodated along border faults and minor internal deformation and volcanic activity; these features are reconciled with the first evolutionary stage. The northern MER has thinner (~30 km thick) crust and is in mature incipient continental rupture, with the deformation focused within the rift and minor activity along border faults, therefore representing the second evolutionary stage (Agostini et al. 2011).

The portions of the rift focusing Quaternary-Recent volcanic and tectonic activity are identified by NNE-SSW striking right stepping en-echelon zones, ~20 km wide and ~60 km long, constituting **magmatic systems**, Most magmatic systems lie within the rift and along its axis, although striking at a slightly oblique angle to the rift axis. Active surface deformation in magmatic systems

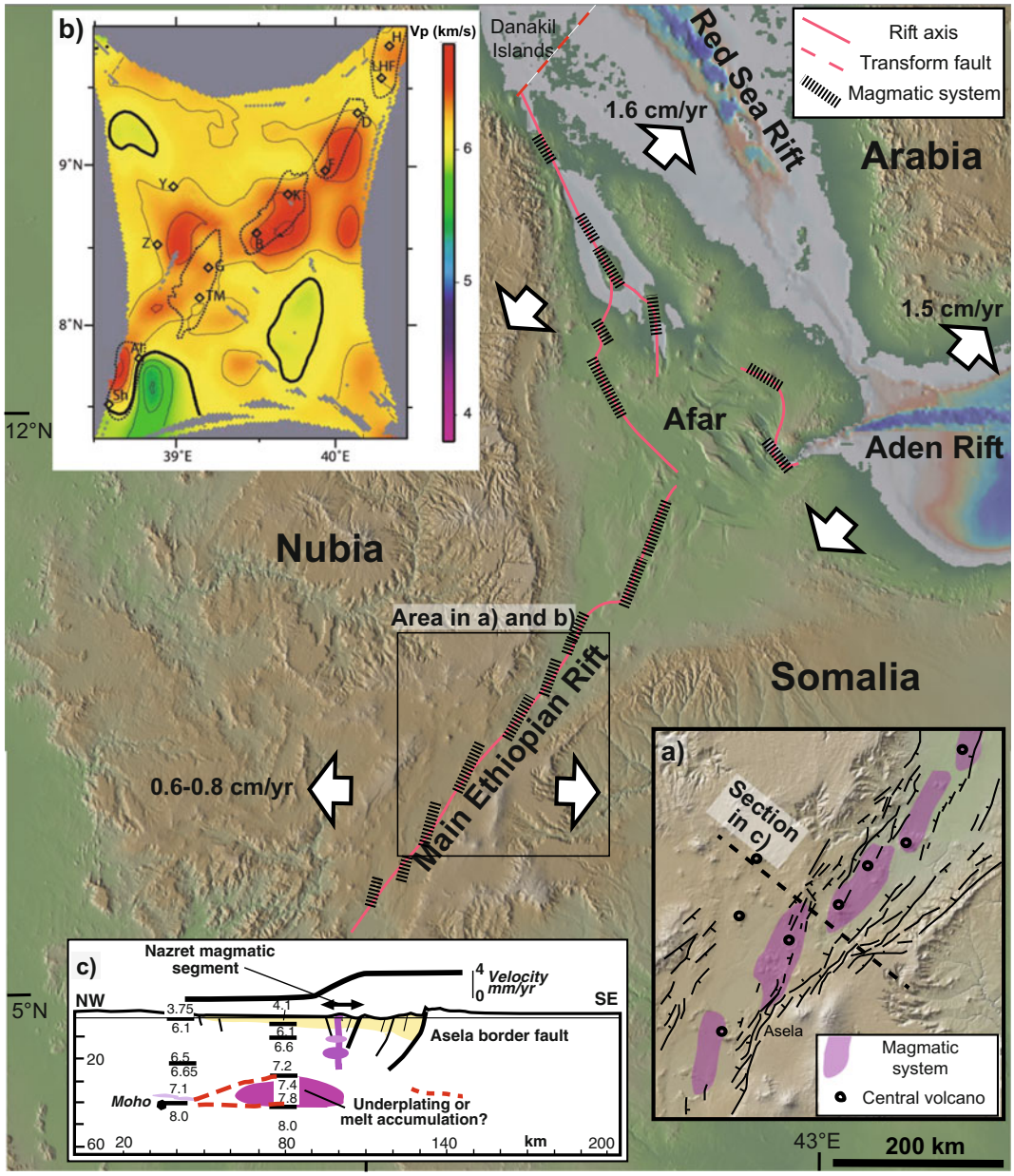

Fig. 11.2 Overview of the Main Ethiopian Rift and Afar triple junction, highlighting the rift axis, magmatic systems and possible transform faults (red dashed line). Insets **a**, **b** enlarge the same area of the MER. Inset a) shows the main magmatic systems, faults and polygenic volcanoes (Ebinger and Casey, 2001). Inset **b** shows velocity anomalies in a horizontal slice at 10 km depth below rift floor; high-velocity (Vp) bodies below rift axis are interpreted as solidified magmatic intrusions; magmatic systems are shown by dotted lines (Keranen et al. 2004). Inset **c** shows a NW–SE trending crustal section of the central portion of the MER (location in **a**); (Ebinger and Casey 2001): numbers represent seismic velocities (in km/s); dot is crustal thickness; bold line above is geodetically determined extensional velocity along line of section (Bilham et al. 1999). Base DEM provided by GeoMapApp

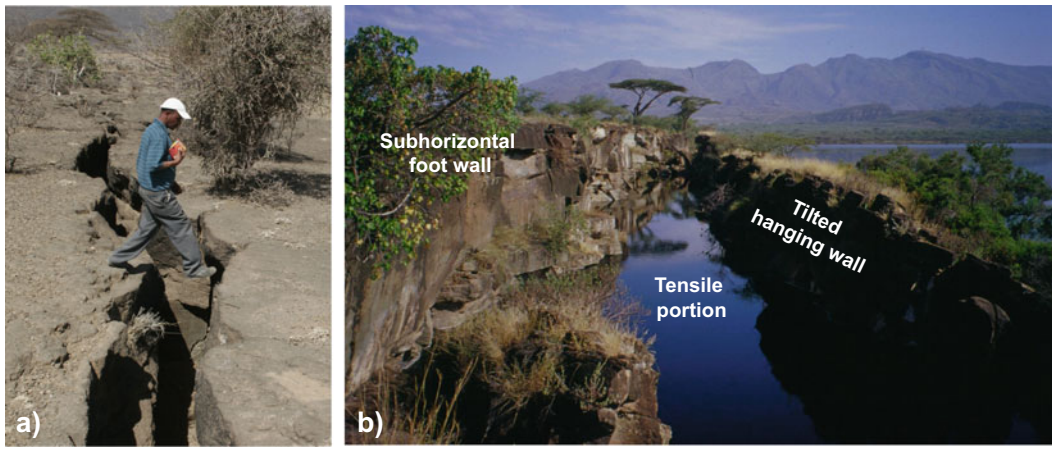

Fig. 11.3 Structural features along the axis of the Main Ethiopian Rift. **a** Extension fracture (photo courtesy Joel Ruch); **b** open normal fault with tilted hanging wall: Fantale volcano is visible in the background, to the north

consists of metres-wide extension fractures and "open normal faults", showing a distinctive tensile portion between their tilted hanging wall and horizontal foot wall (Fig. 11.3). Volcanic activity in a magmatic system includes a dominant polygenic felsic volcano, often with summit caldera, and several mafic monogenic volcanoes, broadly aligned parallel to the system. The magma within the reservoir of the polygenic volcano may intrude laterally (along the system) through dikes, eventually feeding the monogenic fissures, or intrude vertically and erupt within the volcano. In the first case, the mafic primitive composition suggests a provenance of the dikes from the deep, less evolved portion of the magma chamber, or of the reservoir. In the second case, the deeper magma may interact with the felsic magma chamber, differentiating and producing more evolved compositions. The magmatic systems, focusing magmatic and tectonic activity, are responsible for rift opening through dikes mainly at depth and through normal faults and extension fractures mainly at the surface, accommodating more than 80% of the strain across the MER at depths shallower than 10 km (Fig. 11.4; Ebinger and Casey 2001).

Geodetic measurements between 1992 and 2010 suggest that the MER has an overall divergent motion of ~0.7 cm/year along an east–west direction, with a combination of localized high strain rate and adjacent distributed low strain rate zones over a wide range of length and time scales in different settings. In addition, the oblique opening of the Nubian and Somali plates contrasts with the orthogonal opening (NW–SE oriented) of the extension fractures observed along the rift axis, suggesting kinematic partitioning across rift. The geodetic estimates for opening rate are at least one order of magnitude larger than the geological ones over the last ~7 ka, suggesting that, along the rift axis, most extension is accommodated at depth or that the spreading rate is not uniform (Williams et al. 2004; Acocella et al. 2011; Kogan et al. 2012; Birhanu et al. 2016). Geodetic data also highlight deformation of polygenic volcanoes, mainly in the southern MER, as at Corbetti, Aluto and Tullu Moye (Biggs et al. 2011; Greenfield et al. 2019).

Volcanism along the MER is mainly bimodal, with mafic and felsic compositions and scarce intermediate rocks. Fractional crystallization generated zoned magma chambers with felsic melts accumulating at the top and feeding the polygenic volcanoes, often with explosive rhyolitic eruptions generating calderas. Mafic magmas were likely erupted from the bottom of these reservoirs. Considerable volumes of crystal cumulate (>100 km^3) are inferred to be stored beneath these felsic magmatic systems, filling at least 16–30% of the volume generated by crustal extension (Peccerillo et al. 2007; Hutchison et al. 2018). The calderas accompanying the

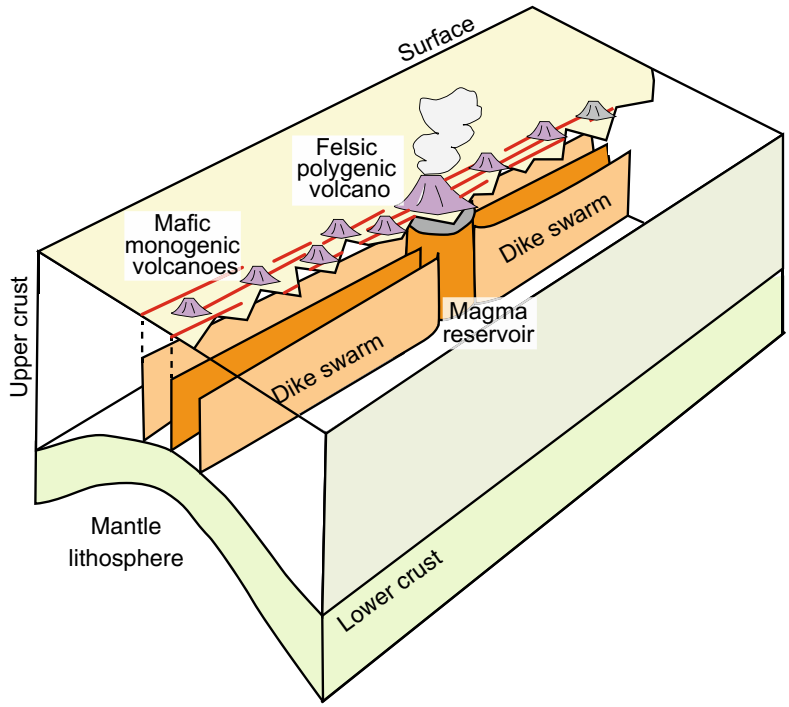

Fig. 11.4 Scheme of a magmatic system along a continental divergent boundary. Magma is fed from a central magma reservoir (cylinder) by dikes propagating mainly laterally in the upper crust (modified after Ebinger and Casey 2001; original image courtesy Cynthia Ebinger)

development of these felsic reservoirs are usually elongated parallel to the extension direction, or to pre-existing regional structures which may be intruded by magma, suggesting in both cases some control of the regional far-field stress. Trachythic volcanism focuses off-rift, likely related to a deeper source, which prevents melts from reaching rhyolitic compositions. The widespread off-rift volcanism, building elongated volcanic edifices up to 1.5 km high, is structurally controlled by the unloading of the rift depression, which alters the local stress field below the rift, steering the magma from beneath the rift axis towards the rift flanks. At a much smaller scale, the activity of normal fault scarps within the rift, responsible for local unloading on their hanging wall, may also explain the clustering of the monogenic vents on their foot wall, at a few hundred of metres from the scarp (Maccaferri et al. 2014, 2015).

At depth, geophysical data show that the crustal thickness along the MER varies between 38 (to the south) and 27 km (to the north) and that of the Ethiopian Plateau to the sides of the rift varies between 44 and 33 km (Mackenzie et al. 2005). The MER at depths between 7 and 25 km hosts pervasive cooled magmatic intrusions, largely dikes, accommodating extension. These intrusions form segmented, ~20 km wide and ~50 km long bodies in a right stepping en-echelon pattern, approximately mimicking the surface segmentation of the magmatic systems. Therefore, rifting obliquity localizes intrusions into the crust within the en-echelon magmatic segments. Seismicity also focuses along the magmatic systems, providing deeper evidence for faulting and diking (Fig. 11.2; Keranen et al. 2004; Dugda et al. 2005; Keir et al. 2006, 2015). At further depth, a segmented low velocity zone suggesting partial melt reaches the upper mantle and extends to the rift sides, connecting northward with low velocity structures under Afar. At even higher depth, this low velocity zone merges with the upper mantle continuation of the plume

(Hammond et al. 2013). Shear-wave splitting in the upper mantle indicates a strong melt-induced anisotropy, supporting a magma-assisted rifted lithosphere. In synthesis, the timing of rift sector development, the three-dimensional focusing of melt, and the ponding of plume material influence intrusions and volcanism along the MER (Bastow et al. 2008; Kendall et al. 2005).

11.3 Transitional Rifts: Afar

The transition between continental and oceanic lithosphere along a divergent plate boundary can be observed, although partly complicated by the activity of the mantle plume, in the Afar area. This area connects the above-mentioned continental MER with the Gulf of Aden and Red Sea oceanic rifts, forming a triple junction, that is where the Nubian, Somali and Arabian plates meet (for an overview see Varet 2018).

The evolution of the Afar area is mainly related to the emplacement of a mantle plume below East Africa. The arrival of the plume head induced a broad uplift of the lithosphere from the late Eocene to the early Oligocene, accompanied by the emplacement and eruption of more than 0.5×10^6 km^3 of flood basalts (Ethiopian Traps), mainly within 1 Ma, at ~30 Ma (Mohr 1983; Hofmann et al. 1997; Furman et al. 2016). In the last ~23 Ma the Arabian-Nubian shield fragmented, separating the Nubian, Arabian and Somali plates along the Gulf of Aden, the Red Sea and the MER, thinning the lithosphere from 100 to 50 km and allowing significant decompression melting. The mean spreading rates of the Gulf of Aden (or Aden) Rift and the southern portion of the Red Sea Rift are ~1.1 to ~1.6 cm/year and ~1.6 cm/year respectively, higher than the 0.7–0.8 cm/year of the northern MER, implying that most of the deformation in Afar results from the activity and interaction of the oceanic Aden and Red Sea rifts (Fig. 11.5; Tapponnier et al. 1990; Vigny et al. 2007; McClusky et al. 2010; Kogan et al. 2012). In the easternmost Aden Rift the onset of seafloor spreading is dated at ~20 Ma, with a

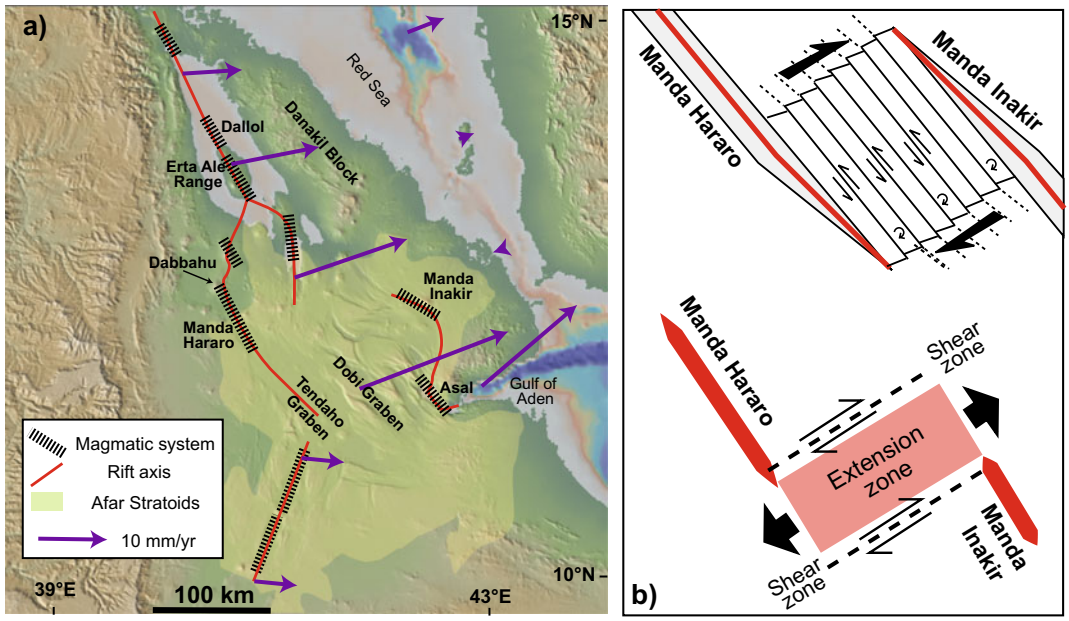

Fig. 11.5 **a** Overview of Afar, highlighting the main magmatic systems, the extent of the Afar Stratoids and the plate motion from GPS measurements: purple arrows show predicted motion on block boundaries (McClusky et al. 2010; base DEM provided by GeoMapApp). **b** End-members kinematic models proposed for central Afar. Top: schematic model of clockwise rotation in central Afar due to "bookshelf" left-lateral faulting between the left-stepping overlapping Manda Hararo and Manda Inakir rifts (modified after Tapponnier et al. 1990). Bottom: schematic model of broadly extending area, delimited by strike-slip fault zones, between the left-stepping overlapping rifts (modified after Pagli et al. 2019)

westward progression. Conversely, in the Red Sea the first pulse of seafloor spreading occurred in its southern part (~17°N), then propagating southwards, separating the Danakil microplate from Arabia, and northwards (Schettino et al. 2016). Below Afar the northward and eastward shallowing of the Moho accompanies increased crustal thinning and segmented melt supply responsible for continental break-up. The thinning shows a northward decrease in the plate strength, in the length of basin-bounding faults, in the length and width of the basins, in the separation of the magmatic centres, and an increase in magma supply, in the volume of Quaternary basalts and the appearance of ~50 to ~80 km long volcanic ridges (Hayward and Ebinger 1996; Bastow and Keir 2011; Gallacher et al. 2016).

Magmatic activity fed by a heterogeneous mantle source has accompanied the recent development of the Afar depression. This recent volcanism can be summarized through 3 main stages (Barberi and Varet 1977; Lahitte et al. 2003; Rooney 2020b). (a) The emplacement of the widespread and more than 1500 m thick "Afar Stratoids" sequence, made up of flood basalts and ignimbrites, underlain by large amounts of silicic lava, marking a major magmatic phase during continental break-up, from 4 to 1 Ma. This trap-like sequence covers approximately two thirds of central Afar, indicating widespread volcanism (Fig. 11.5). (b) The development of polygenic silicic volcanoes, as precursors to rift propagation in the last 2 Ma, prior to the main extensional phase associated with basaltic fissure eruptions. These evolved volcanoes and associated magma chambers form zones of localized lithospheric weakness, concentrating stress and guiding the development of fissure eruptions (Fig. 11.6). (c) The late Quaternary oceanic-type basaltic volcanism, mainly occurring through fissure eruptions along the magmatic systems of the active onland portions of the Red Sea and Aden rifts. The repeated and predominantly intrusive events of the last decades, whose overview is summarized in Fig. 11.7, highlight the current activity of these same axial portions.

The structure of the Afar region is presented in more detail below.

The ~WSW–ENE trending Aden Rift is highly oblique, showing an overall NE-SW

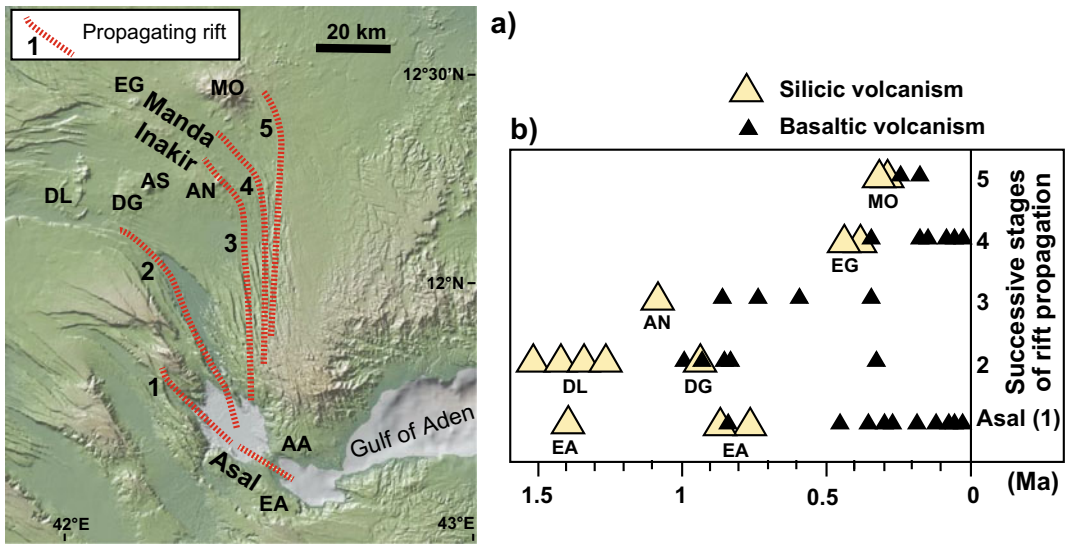

Fig. 11.6 **a** Simplified structural evolution of the onland portion of the Aden Rift in eastern Afar, showing the five successive stages (numbered) of propagation of the Asal Rift to the Manda Inakir Rift. **b** Distribution of silicic (large yellow triangles) and basaltic (small black triangles) volcanic activity as a function of time for the main rift segments associated with the propagation of the Aden ridges; location of volcanoes identified by acronyms is shown in a) (modified after Lahitte et al. 2003). Base DEM provided by GeoMapApp

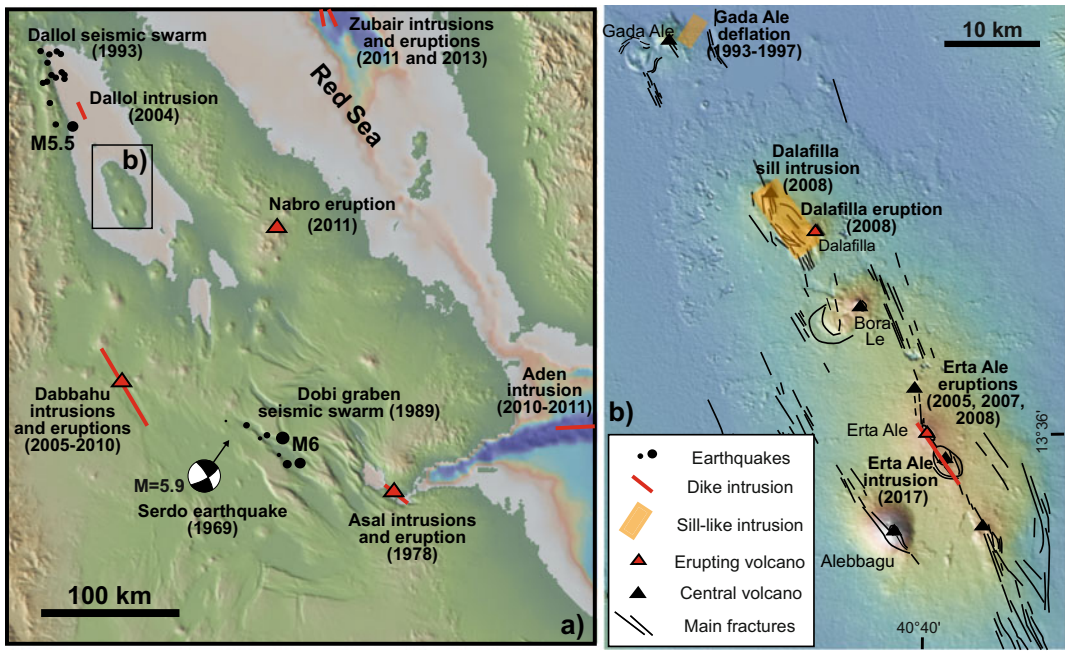

Fig. 11.7 **a** Overview of the magmatic and seismic (approximate location, maximum magnitude reported; from Jacques et al. 1999; Nobile et al. 2012) activity of Afar in the last decades; **b** detail of the recent activity along the Erta Ale Range, Red Sea Rift; see text for details. Additional diking events (not indicated here) occurred in 2000 at the junction between Afar and the northern MER, a few tens of kilometres to the south of the map (Keir et al. 2011) and in 2007 at Jebel at Tair Island, 50 km to the northwest of the Zubair Islands in the southern Red Sea (Jonsson and Xu 2015). Base DEM provided by GeoMapApp

extension direction. This oceanic rift is segmented, with ~E–W trending spreading centres interrupted by NE-SW trending transform faults. One of the easternmost segments experienced an event of seafloor spreading related to the lateral propagation of a dike from November 2010 to March 2011. This dike, responsible for widespread seismicity with magnitude clustering between 2.1 and 5.6, produced an estimated horizontal opening between 0.6 and 2.9 m (Ahmed et al. 2016). The onland continuation of the Aden Rift consists of the NW–SE trending Asal-Ghoubbet Rift and, to the north, the parallel but offset Manda Inakir Rift (Fig. 11.5). These two magmatic systems are connected by a transfer zone forming an extensional faulted monocline due to crustal downwarping undergoing rotations of small rigid blocks about a vertical axis. Each magmatic system consists of subvertical to riftward-dipping active normal faults and an axial portion of active tensile fracturing and volcanic activity, with fast fault propagation and block rotation rates, implying transient strain transfer (Tapponnier et al. 1990; Manighetti et al. 2001). The Asal magmatic system underwent a rifting episode in 1978, due to the along emplacement of a 4.5 km long and 2.2 m thick dike accompanied by widespread seismicity and eruption at Ardoukoba, in the northwest part. At the same time, a ~8 km long and ~4 m thick dike emplaced below the offshore Ghoubbet Rift, ~15 km to the southeast. The emplacement of these dikes was associated with the deflation of the mid-segment Fieale caldera, suggesting that its magmatic reservoir laterally fed the dikes and the eruption (Tarantola et al. 1979; Smittarello et al. 2016; Fig. 11.7). Between 1978 and 1986 the Asal Rift opened at a

fast rate, mainly magmatically and aseismically, whereas after 1986 the opening rate and seismicity decreased. Over more than 23 years following the stretching episode, the Asal Rift has sustained mass input and post-rifting unsteady opening, higher than the large scale Arabia-Somalia motion. The InSAR data from 1997 to 2005 show slip along the Asal Rift faults, suggesting that these are in a critical failure state and respond instantly to small fluid pressure changes. More generally, the whole fault activity and distribution along the Asal Rift appears dike-controlled (Doubre et al. 2007; Vigny et al. 2007; Pinzuti et al. 2010).

Northern Afar is built on the onland appearance of a segment of the Red Sea Rift propagating southwards, probably promoting an incipient transform fault passing through the Danakil Islands (Fig. 11.2). The onland portion of the Red Sea Rift consists of two main NW–SE trending en-echelon segments, nearly 500 km long (Fig. 11.5). The northern segment separates the Ethiopian Plateau, on the Nubian plate, from the Danakil Block, or microplate, which experienced an overall eastward shift and counter clockwise rotation. The crust in between these plates, lying below sea level, is thinner ($\sim$15 km thick) than the average crustal thickness of Afar ($\sim$25 km), suggesting an advanced, proto-oceanic rifting stage (Eagles et al. 2002). To generate such a large amount of subsidence, upper-crustal extension should be dominated by faulting, coupled with ductile extension at depth, and only locally by magmatic intrusions. Here seismicity focuses along the rift axis and the western marginal graben. The former occurs in conjunction with magmatic intrusion, while the latter is either caused by upper crustal faulting accommodating crustal thinning or by flexural faulting between the rift and plateau (Bastow et al. 2018). The most dramatic manifestation of volcanic activity along the northern portion of the onland Red Sea Rift is the Erta Ale Range, consisting of largely basaltic $\sim$NW–SE aligned central volcanoes, fissure eruptions and hydrothermal spots, associated with fracturing and diking. Here InSAR and seismicity data have spotted repeated activity: this includes episodes of magma withdrawal at Gada Ale volcano between 1993 and 1996, along-rift dike emplacement below the Dallol hydrothermal spot in 2004, sill deflation below Dalafilla volcano in 2008 and along-rift dike propagation in 2017 below Erta Ale caldera, which hosts a long-lasting lava lake (Fig. 11.7; Barberi and Varet 1970; Amelung et al. 2000; Nobile et al. 2012; Pagli et al. 2012; Xu et al. 2017).

To the south, the onland portion of the Red Sea Rift branches into the Tat'Ali Rift and, to the west, the more developed NW–SE trending Manda Hararo Rift, which reaches the NW–SE trending Tendaho Graben into central Afar. The upper crust below the Manda Hararo Rift has the most significant low velocity dispersion anomalies and highest conductivities of Afar. The conductivity anomaly has been interpreted to indicate that more than 500 km^3 of magma is present, mainly near the crust-mantle boundary. The volume of magma is potentially sufficient to feed crustal intrusions tens of thousands of years (Buck 2013; Desissa et al. 2013). A rifting episode occurred at Dabbahu, in the northern Manda Hararo Rift, from 2005 to 2010. The major intrusive event, in 2005, emplaced at least two laterally propagating dikes, up to 8 m thick, over a length of 60 km from a source below the Ado'Ale volcanic complex, in the centre of a magmatic system with the dikes at a depth between 2.5 and 10 km. This event was accompanied by a minor eruption, magnitude $M > 5$ earthquakes and surface deformation with normal fault displacement of up to 3 m and extension fractures (Fig. 11.8; Wright et al. 2006; Rowland et al. 2007; Ayele et al. 2009). Normal fault reactivation during this event suggests that the faults along the rift axis result from the upward propagation of the stress during diking and thus magma may be responsible for the relief of the magmatic system. Thirteen more dike intrusions, for a total volume of magma larger than 3 km^3, occurred between 2005 and 2010. Their cumulative opening becomes largest in the central part of the intrusion, where smoothing deficits from the first intrusion were observed. Most dikes were again sourced from the centre of the magmatic system. During these diking events, the seismicity was largely released at the dike tip, during dike

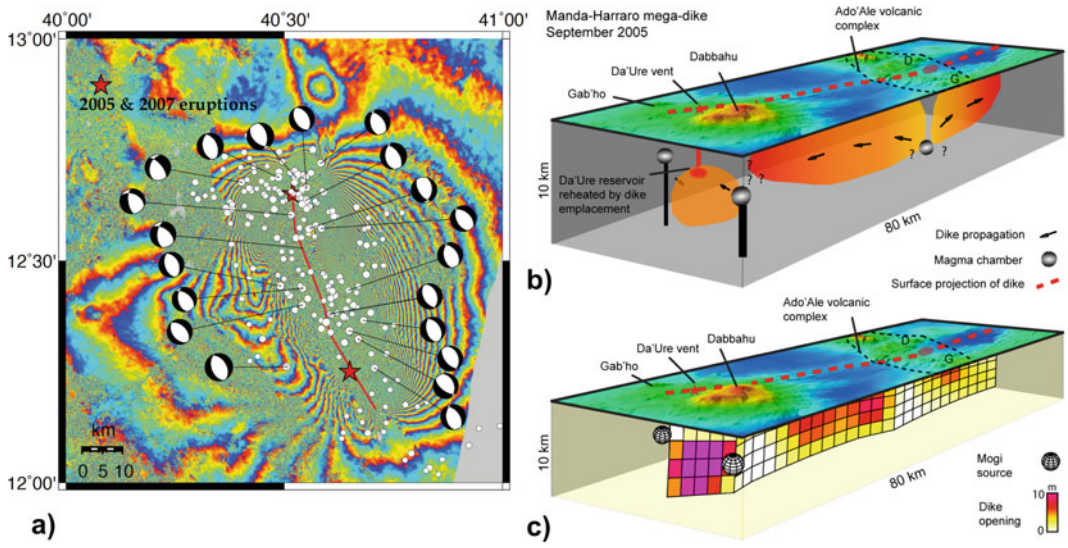

Fig. 11.8 The 2005–2010 Dabbahu rifting episode, Afar (Ayele et al. 2009). **a** Fault plane solutions of earthquakes during the onset of the rifting cycle in the Dabbahu-Manda Hararo segment between September 4–October 4, 2005. Solutions are superposed on an interferogram formed by satellite radar images acquired on May 6 and October 28, 2005. Red stars indicate sites of the 2005 silicic eruption and the 2007–2009 fissural basalt eruptions. **b** Scaled model for the September 2005 intrusive event. Red dashed line indicates the surface trace of the dikes. Arrows indicate magma movement directions. **c** Topography and model of dike opening that reproduces vertical and horizontal crustal movements determined from InSAR data, constrained by seismic observations. Spheres are Mogi sources that simulate magma pressure sources added to the dike opening to produce the observed surface deformation patterns

propagation. These diking events are followed by a decadal-scale period with extension rates faster than the secular divergent plate motion, as observed in the Aden Rift (Fig. 11.9; Ebinger et al. 2010; Belachew et al. 2011; Pagli et al. 2014). Integrated studies reveal that, on the longer-term, an intrusive episode like that observed at Dabbahu between 2005 and 2010 has occurred roughly every 10 ka. More generally, the 2005 intrusion at Dabbahu has confirmed the importance of

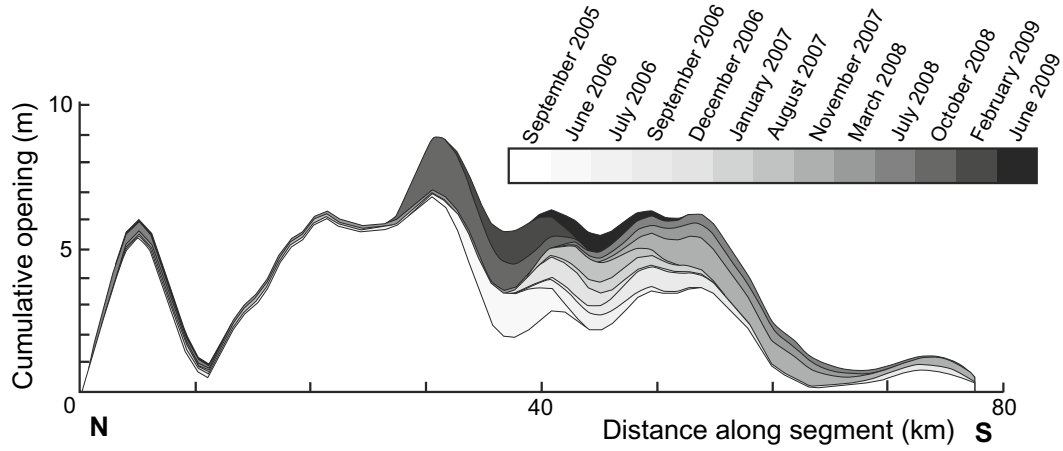

Fig. 11.9 Depth-averaged dike opening from 2005 to 2009 for the top 10 km of the crust beneath the Dabbahu-Manda Hararo segment plotted against distance along the segment from north to south (modified after Ebinger et al. 2010)

episodic and rapid magma emplacement in the opening of a rift and thus in plate boundary deformation (Sigmundsson 2006a; Medynski et al. 2016). This event has been strengthened by the successive dike intrusions, highlighting how focused accretion at magmatic systems occurs through lateral magma propagation. Therefore, the Dabbahu episode has shown that, while tectonic forces may prepare or encourage rifting over longer-time scales (thousands of years), magmatic injection promotes major rifting episodes lasting shorter time spans (years).

The Manda Hararo Rift terminates into the Tendaho Graben, which formed in the last ~1.8 Ma and abruptly interrupts the MER structures. The Tendaho Graben is several tens of kilometres wide and a few hundred kilometres long, and hosts eruptive fissures and central volcanoes. The graben is the southernmost expression of the onland portion of the Red Sea Rift and experienced a decrease in tectonic and magmatic activity once the Aden Rift appeared onland, suggesting a mutual interdependence in the activity of these two rifts. Its distinctive structure with inward tilted margins may result from two main magma-related processes: (a) the collapse induced by magma withdrawal during the eruption of the voluminous Afar Stratoids from the graben axis, showing how large and repeated fissure eruptions form collapsed rifts; (b) the load of the axial mafic intrusions in a thinned and heated plate that decreases its strength (Acocella 2010; Corti et al. 2015). The Tendaho Graben is the largest of a series of NW–SE trending basins in central Afar, between the Manda Hararo and the Asal-Ghoubbet-Manda Inakir rifts. This area is characterized by pervasive faulting, developing tens of rigid blocks separated by ~NW–SE striking faults whose kinematics may be consistent with two main models (Fig. 11.5). (a) A bookshelf faulting model, based on the reactivation of the NW–SE trending normal faults as left-lateral structures, due to the interaction between the Aden and Red Sea overlapping rifts: this is consistent with the measured clockwise rotations of crustal blocks about a horizontal axis in the last 1.8 Ma in central Afar. A modification of this bookshelf model, based on seismicity data, emphasizes the current extension of the NW–SE trending faults (Tapponnier et al. 1990; Sigmundsson 1992). (b) An overall distributed extension on rift parallel normal faults, driving rift perpendicular shearing at the tips of spreading rifts and finally achieving plate boundary linkage during incipient seafloor spreading. The geodetic behaviour of this extended area highlights a central microblock evolving separately from the three surrounding plates, although depending on the availability of magma supply within the nearby rifts (Doubre et al. 2017; Pagli et al. 2019). These two models are not mutually exclusive, as the former relies mainly on paleomagnetic data in the last ~2 Ma and the latter on present-day seismicity and geodetic data.

11.4 Oceanic Rifts

Prolonged extension leads to further lithospheric thinning and the progressive formation of new oceanic crust, which is produced at an oceanic ridge along the plate boundary. Here extensional stress accumulates at a steady rate, to be episodically released in discrete events of magma intrusion, volcanism and associated faulting, whose magnitude is proportional to the time elapsed since the last event. The prolonged activity of an oceanic ridge is responsible for **seafloor spreading**, that is the formation of new oceanic crust through magmatic activity.

Oceanic ridges are segmented features: their continuity is most notably interrupted by transform faults or overlapping spreading centres (Fig. 11.10). **Transform faults** are hard-linkage transverse structures, striking parallel to the spreading direction of the two plates and connecting offset ridge segments. Because of the opposite sense of motion of the plates between the two offset ridges, transform faults display predominant strike-slip kinematics. This motion may extend also outside the zone between the ridge segments, along fracture zones, provided that the ridge segments have different spreading velocity. **Overlapping Spreading Centres** are soft-linkage interaction zones between the extremities of oceanic ridges, showing an overlapping zone with

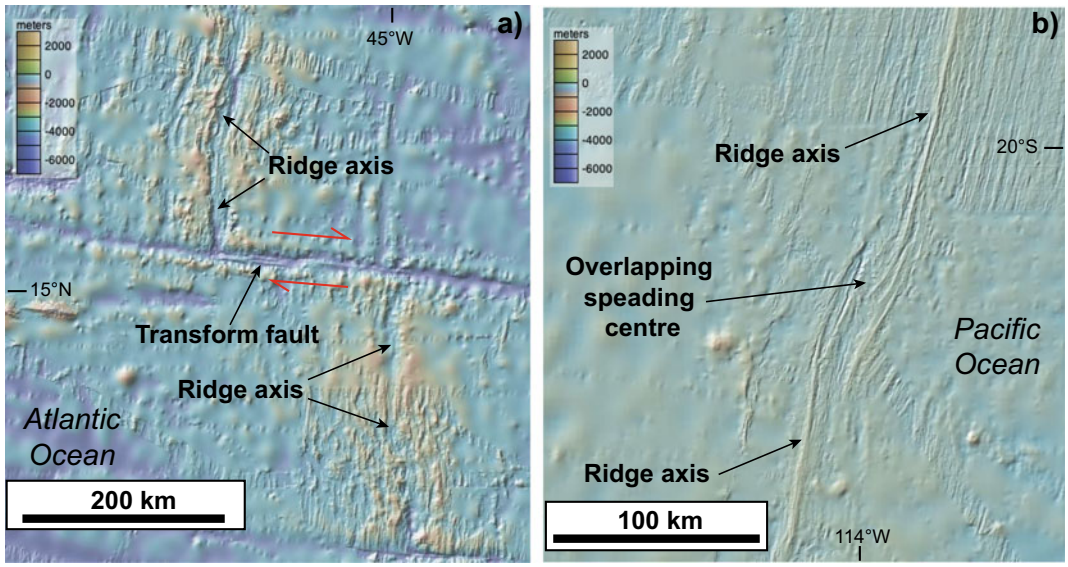

Fig. 11.10 Types of linkage between segmented oceanic ridges. **a** Hard-linkage, through a transform fault; red arrows show the relative motion along the fault. **b** Soft-linkage, through an overlapping spreading centre. Base DEM provided by GeoMapApp

characteristic hook-shaped geometry explained by the variation in the ridge propagation force as two ridges approach and pass each other (e.g., Pollard and Aydin 1984). The segments of the oceanic ridges present a four-order hierarchy. At higher orders, segments are shorter (less than 10 km for fourth-order and up to 1000 km for first-order) and more short-lived (from 10^2 to 10^4 years for fourth-order to 10^7 years for first-order; Macdonald et al. 1991). First-order ridge segments are limited by transform faults, whereas second-order segments terminate at Overlapping Spreading Centres. Several hypotheses may explain the segmentation and along-strike propagation of the ridges, as summarized below (Macdonald et al. 1991; Vanderbeek et al. 2016). Oceanic ridges may be divided into stable spreading cells, each several tens of kilometres long, linked to uniformly spaced Rayleigh–Taylor gravitational instabilities in the upper mantle; in this model, ridge segmentation is driven by mantle buoyancy. Alternatively, oblique mantle flow beneath the ridges may reorient the spreading segments and promote ridge-axis discontinuities; these would decrease the efficiency of upward melt transport, thus defining segment scale variations in magmatic processes. Gravitational spreading forces due to excess ridge axis topography, where the elevation of the axial region of the ridge above its flanks represents gravitational potential energy, may also promote along-strike growth; this model works well where hot spot magmatism has produced significant ridge axis elevations and variations in near-field stress. Another mechanism is related to the crack propagation force caused by far-field plate stresses, similar to what observed in fracture mechanics, where the propagation force at the crack tip increases with crack length, with the longer segment lengthening at the expense of the shorter; this mechanism may explain why long ridge segments tend to lengthen and prevail over shorter neighbouring segments. Finally, changes in spreading direction may also provide a mechanism for propagation and segment lengthening, although the force to drive ridge propagation is limited.

Depending upon their spreading velocity, ridges are classified as **ultrafast** (full spreading rate of >12 cm/year; as the fast portions of the East Pacific Rise), **fast** (<12 to >8 cm/year; as the slow portions of the East Pacific Rise), **intermediate** (<8 to >5 cm/year, as the Juan de Fuca Ridge, in the north Pacific), **slow** (<5 to >2 cm/year; as the Mid-Atlantic Ridge), and **ultraslow** (<2 cm/year, as the Southwest Indian

Ridge; Fig. 11.11). The spreading rate strongly influences the extent of mantle melting beneath the ridge, magma supply, hydrothermal heath loss and crustal deformation, although the extent of mantle melting may also depend on along-axis variations in the mantle temperatures and/or mantle chemistry (Michael et al. 2003). In general, faster ridges are more linear, with axial rise and narrow (less than 1 km) and elongated summit depression. Their higher magmatic productivity is supported by a continuous and shallower (approximately 1 km of depth) axial melt reservoir, resulting in frequent, relatively homogeneous and small volume eruptions. Faster ridges thus tend to approach spatially and temporally uniform along-axis mantle flow, with fluctuations of the along-axis characteristics considerably more subdued than at slower ridges. Conversely, slower ridges are more tortuous, with a deeper and wider (several kilometres) axial depression or graben, bordered by faults with higher displacement-length ratios associated with uplifted shoulders. Their magmatic productivity results from discontinuous, unstable and deeper (approximately 3 km of depth) melt pockets, feeding infrequent, heterogeneous and larger volume eruptions, also off-rift. At the end of the spectrum, ultraslow ridges are

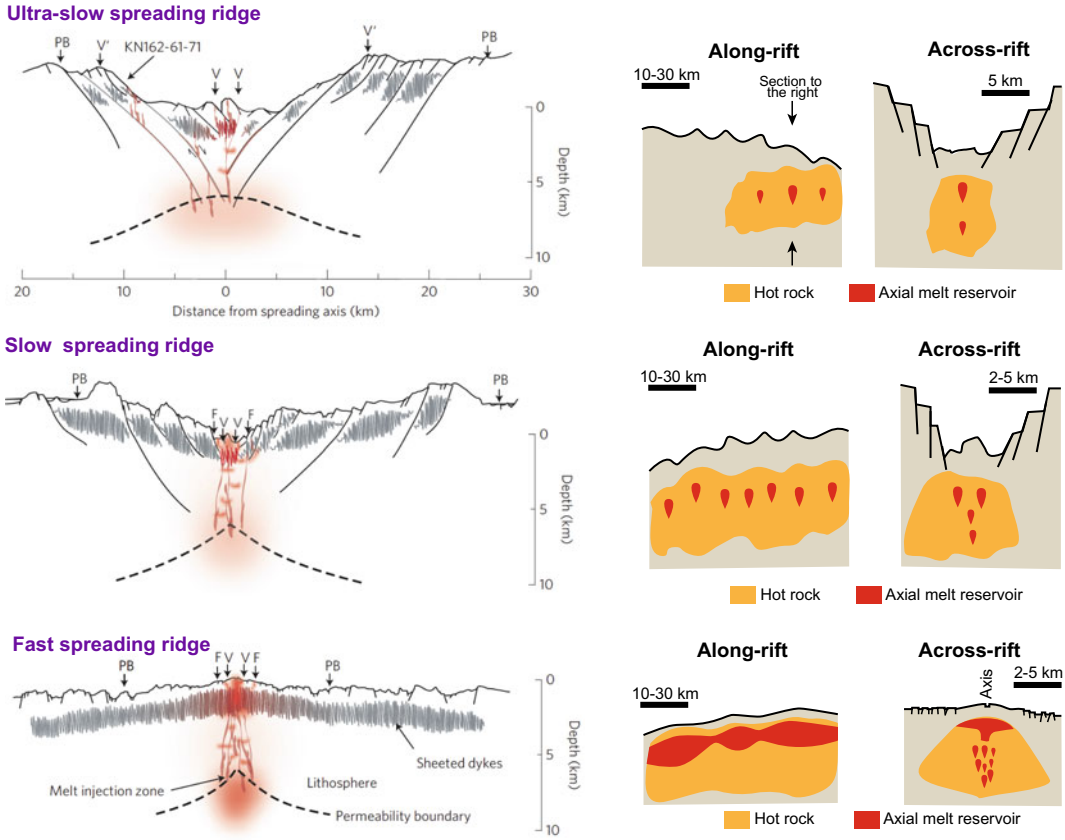

Fig. 11.11 Left: cross-axis bathymetric profiles for ultraslow, slow and fast spreading ridges, including the neovolcanic zone (V), the zone of fissuring (F) and the plate boundary zone (PB, active faulting). The intensity and width of the melt injection zone (red; that is, melt volume) and the thickness of the sheeted dikes (grey lines; dike focusing) indicate the robustness of melt generation and the relative roles of magmatic versus tectonic accretion during extension (modified after Standish and Sims, 2010). Right: schematic enlargements to show fine-scale segmentation of along- and across-rift sections for the ultraslow, slow and fast spreading examples (modified after Macdonald et al. 1991)

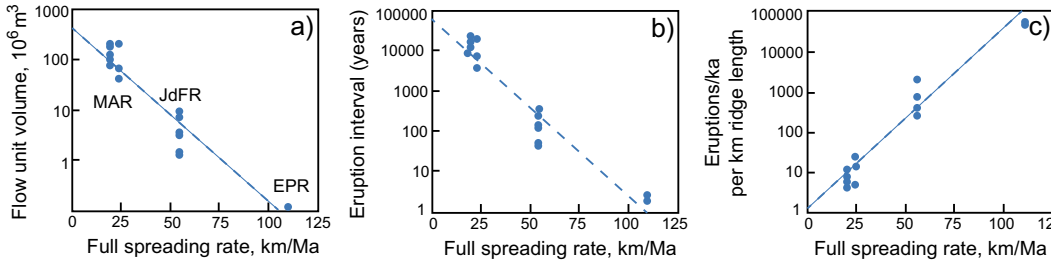

Fig. 11.12 Temporal and spatial intervals and volumes of eruptions against spreading rate (MAR: Mid-Atlantic Ridge; JdFR: Juan de Fuca Ridge; EPR: East Pacific Rise; Perfit and Chadwick 1998)

characterized by non-magmatic portions, where regional tectonic activity dominates (Fig. 11.12; Macdonald et al. 1991; Purdy et al. 1991; Calvert 1995; Niu and Hekinian 1997; Macdonald 1998; Perfit and Chadwick 1998; Sibrant et al. 2018). These features may also affect the seismic behaviour, as in faster ridges most fault slip seems to occur with minor seismicity or aseismically, and in slower ridges seismic slip may represent most of the total fault displacement. This possible diverse behaviour may result from the different thickness of the seismogenic zone, which is proportional to the seismicity during fault slip: this zone, being smaller in faster oceanic ridges, may produce a lower seismic slip (Mark et al. 2018).

Differences in the magmatic input to dikes, driven by the spreading rate, may significantly contribute to the observed differences in fault patterns along slow and fast ridges. Where magma supply is continuous and robust (steady state), volcanic output dominates over regional tectonic processes, which are largely aseismic, along ridge segments typically 100–1000 km long. Where the supply is intermittent (non-steady-state), regional tectonic activity, largely associated with seismicity, may dominate along ridge segments typically 50–80 km long, with deep earthquakes, major normal faults and exposures of lower crustal rocks. The critical spreading rate between steady-state and non-steady-state supply is inferred to be 5–6 cm/year (Mutter and Karson 1992; Perfit and Chadwick 1998; Sandwell and Smith 2009). However, investigations on the intermediate spreading Costa Rica Rift reveal that its evolution is also sensitive to relatively small changes in the full spreading rate. These fluctuations correspond to different processes occurring at the ridge axis, so that even at intermediate spreading ridges there appear to be two end-member modes of crustal formation: one magmatic, occurring at the faster end of the spectrum, and the other magma-dominated, but accompanied by enhanced tectonic extension that occurs at the slower end. These magma-dominated and faulting-enhanced modes of spreading are not mutually exclusive, as the oceanic crust can form via their combination, with varying predominance and/or durations of each, resulting in a fine balance. These modes of spreading may be influenced by tectonic events associated with the plate boundary, changes in the spreading rate, or patterns of spreading of adjacent plates (Wilson et al. 2019).

The spreading rate is thus a crucial parameter in controlling the morphology, structure, magmatic supply, productivity and eruptive frequency of oceanic ridges. This parameter in turn may also depend on the general far-field tectonics at the other ends of the oceanic lithospheric plates, that is along subduction zones. Not only this condition modulates the spreading rates, but it also alters the convection regime by obstructing the circulation of plates, which in turn modifies the surface kinematic conditions for the convecting mantle. Therefore, the spreading rate of a ridge may mirror its status in the global plate tectonics framework (Husson et al. 2015).

The main features of ultraslow (Sect. 11.4.1), slow (Sect. 11.4.2) and fast and ultrafast (Sect. 11.4.3) oceanic ridges are discussed below, considering representative examples.

11.4.1 Ultraslow Ridges: The Red Sea and the Southwest Indian Ridge

Ultraslow spreading ridges, characterized by a full spreading velocity lower than 2 cm/year, have been recently recognized as an important class of oceanic ridges, also sharing similarities in the processes that govern the break-up of continents along non-volcanic rifted margins (Snow and Edmonds 2007). Ultraslow ridges consist of linked magmatic and amagmatic accretionary segments, the latter being a previously unrecognized class of accretionary plate boundary structure. As a result, these ridges can produce magmatic crust or exhume (i.e., bring to the surface) highly serpentinized peridotite from the upper mantle to the seafloor (Dick et al. 2003; Schlindwein and Schmid 2016; Grevemeyer et al. 2018; Reston 2018). Exhumation occurs through oceanic low-angle, or detachment, faulting, which may be a major mode of seafloor accretion also at some slow ridges. This is associated with dramatic changes in seafloor morphology, as detachments form expansive dome structures with corrugated surfaces, known as oceanic core complexes. These areas lack shallow seismicity in the upper 15 km of the lithosphere, but unusually contain earthquakes down to depths of 35 km, implying a cold, thick lithosphere. The detachments often transition laterally to segments producing magmatic crust, consisting of multiple regularly-spaced normal faults that form volcanic abyssal hills parallel to the spreading axis. These magmatic regions thin dramatically under volcanic centres, allowing along-axis melt flow. The switch between magma-rich and magma-poor oceanic crustal accretion is attributed to along-axis gradients in lithospheric strength or, more likely, magma supply. Indeed, highly punctuated volcanism active for tens of millions of years suggests that first-order ridge segmentation is controlled by stable mantle processes of melting and melt segregation, with mantle temperatures varying significantly along-axis suggesting that the extent of mantle melting is not a simple function of the spreading rate. The transition from slow to ultraslow ridges may also be independent of melt productivity, and rather result in the efficiency of vertical melt extraction (Jokat et al. 2003; Michael et al. 2003; Montesi and Behn 2007).

Examples of ultraslow spreading ridges include the Mid-Cayman spreading centre (Caribbean), the Gakkel Ridge (Arctic Ocean), the Red Sea and the Southwest Indian Ridge; the last two cases are described below.

Considering the Red Sea allows completing the regional continuum from continental (MER) to transitional (Afar) and oceanic plate divergence. Moreover, the Red Sea displays lithosphere that is in transition from rifting to seafloor spreading, providing the opportunity to describe incipient oceanic floor formation. The Red Sea is in fact a newly-formed oceanic rift with only parts having entered the seafloor spreading stage. Magnetic data suggest that the Red Sea has been widening from 0.7–0.8 to 1.6 cm/year at the northern and southern portions, respectively, consistent with geodetic constraints of current opening at 0.7 and 1.5 cm/year (Fig. 11.13; Bosworth et al. 2006; Almalki et al. 2015). After a first rifting pulse at ~34 Ma, the southern portion of the Red Sea started to open at ~26 Ma, soon after the eruptive climax of the Ethiopian Traps. A first phase of axial spreading created oceanic lithosphere between ~26 and ~24 Ma, propagating segments of oceanic crust northward above areas of localized rise of mantle melts, fading into steady passive crustal accretion with slower spreading: rifting, rift flank uplift and volcanism occurred nearly simultaneously (Bonatti 1985; Omar and Steckler 1995; Ligi et al. 2011; Almalki et al. 2015, and references therein). Then, between 22 and 6 Ma, localized extension and mafic diking at the edge of the Arabian platform heralded a pause in oceanic basin formation and a shift in the locus of extension from the central spreading ridge to the eastern continental–transitional crust zone. Re-initiation of ridge activity and spreading occurred at ~5 Ma, resulting from a plate reorganization attributed to the switch from subduction to collision and oblique motion between Eurasia and Arabia, driven by the extrusion tectonics in Anatolia, which allowed

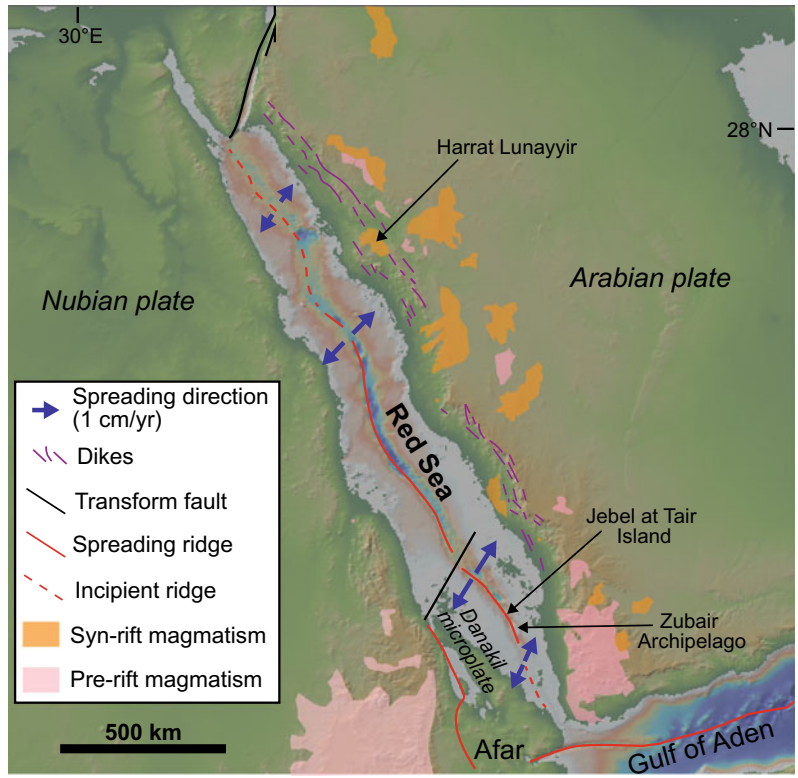

Fig. 11.13 Main tectono-magmatic features of the Red Sea area, illustrating the opening vectors, the spreading ridges in the southern part and the incipient ridges in the northern part, as well as the main volcanic products erupted before (mainly Oligocene) and during rifting (modified after Almalki et al. 2015). DEM provided by GeoMapApp

renewed and faster motion of Arabia relative to Africa (e.g., Cochran 1983; Almalki et al. 2015). Nevertheless, such a discontinuous and episodic ridge spreading activity in the southern Red Sea indicates a limited role in accommodating crustal extension.

This two-stage spreading model is applicable to the southern and perhaps the central Red Sea, whereas in the less extended northern Red Sea diffuse extensional models are better applicable, because there is debated evidence for the existence of magnetic stripes and any oceanic crust. The current Red Sea can be thus separated into three distinct portions. The southern Red Sea, experiencing seafloor spreading, or drifting. The northern Red Sea, still largely experiencing continental rifting, with thinning continental crust, intruded mafic melts and limited oceanic crust and seismicity. The central Red Sea, a transition zone where isolated bathymetric deeps mark the oceanic onset of divergence (Bonatti 1985; Ligi et al. 2011, 2019; Mitchell and Park 2014; Schettino et al. 2016; Mitchell and Stewart 2018). These variations may be ascribed to the rheologically weaker behaviour of the southern Red Sea under the influence of the nearby Afar plume, which started the Red Sea rifting (Almalki et al. 2015).

Red Sea tectonic models consider both asymmetric and symmetric extension. Asymmetric extension has been proposed based on simple shear along a regional scale low angle normal fault that breaks away at the surface on the African continent and projects to sublithospheric levels beneath the Arabian plate. This model was used to explain the asymmetric distribution of volcanic rocks along the edge of the Arabian plate and the higher topography on the Arabian side of the Red Sea (Fig. 11.13). However, such a structural asymmetry has not been confirmed by geological or geophysical data (Wernicke 1985; Almalki et al. 2015, and references therein). Indeed, there is an overall difficulty in applying tectonic models, as none of the

models proposed so far is applicable to the entire Red Sea basin.

The lithospheric thickness along the eastern margin of the Red Sea varies considerably, suggesting an important role of asthenospheric flow related to the significant off-rift magmatism on the Arabian side, the last event being the non-eruptive Harrat Lunayyir (Saudi Arabia) dike intrusion in 2009, associated with seismicity and surface fracturing. The dike rose from 10–11 km of depth and almost reached the surface, forming two diverging fracture zones, whose distance increase is due to the progressive deepening of the dike top (Pallister et al. 2010; Chang and Van der Lee 2011; Trippanera et al. 2019).

Volcanic activity has been recently focusing in the southernmost part of the Red Sea. The first volcanic eruption known to occur in the southern Red Sea in over a century started on Jebel at Tair Island in September 2007. The Jebel at Tair activity was followed by two more eruptions within the Zubair Archipelago, about 50 km to the southeast, in 2011–2012 and 2013, both of which started on the seafloor and resulted in the formation of new islands. In particular, the 2011 eruptive event was fed by a 12 km long dike parallel to the Red Sea axis, associated with seismicity and normal faulting, which fed a submarine and then a subaerial eruption. These eruptions suggest that this portion of the Red Sea, where the evidence for a linear spreading centre disappears, is magmatically more active than expected (Jonsson and Xu 2015; Xu et al. 2015; Eyles et al. 2018).

The ultraslow Southwest Indian Ridge allows considering the transition from quasi-melt-free detachment-dominated spreading to magmatic spreading near prominent axial volcanoes. Detachments extend along-axis for several tens of kilometres, with lifetime of ~0.6 to ~1.5 Ma. Once a detachment becomes inactive, the successor cuts into its predecessor's foot wall with opposite polarity, causing part of the foot wall lithosphere to experience further deformation, hydrothermal alteration and, possibly, sparse magmatism (Fig. 11.14). The accretion of the oceanic lithosphere therefore occurs over the lifetime of successive detachment faults with flipping polarity. The transition from this nearly amagmatic detachment-dominated mode to the more common magmatic mode of spreading occurs over along-axis distances of a very few

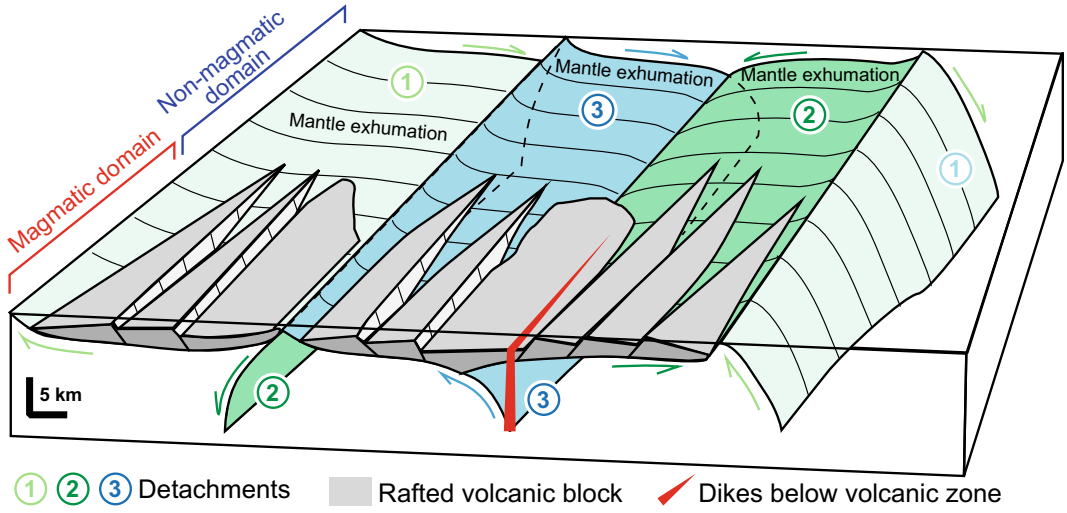

Fig. 11.14 Tectonic model of ultraslow seafloor spreading applied to the Southwest Indian Ridge. Mantle (shown transparent) is in general exhumed to form smooth seafloor by slip on successive detachments with alternating polarity: light green (1) to dark green (2) and then blue (3), the only currently active in the diagram. Block arrows show movement direction. The detachments continue laterally also beneath rafted volcanic blocks (grey; foreground), where increasing magmatic contribution to divergence occurs (modified after Reston 2018)

tens of kilometres. As the magmatic contribution to divergence increases, this transition involves a significant thinning of the axial lithosphere and a gradual decrease of the amount of displacement on faults. Axial magma chambers below the Southwest Indian Ridge have been imaged between 4 and 9 km of depth, suggesting that the ~10 km thick crust is mainly formed by magmatic process. Here magma fills the gap between the diverging plates, thus reducing fault activity and modifying the thickness, thermal state and rheology of the plate boundary. Increased magmatic divergence requires the detachments to root at shallower depths, consistent with the seismicity-defined shallowing of the base of the brittle lithosphere moving along the ridge axis towards the volcanic centres (Jian et al. 2017; Reston 2018; Cannat et al. 2019). The activation of the magmatic or of the detachment-dominated modes of spreading depends on the volume of magma supplied per increment of plate separation and the rheology of the axial lithosphere. Magmatic accretion is not confined to a narrow central spreading axis, as indicated by the young volcanic eruptions broadly dispersed throughout the rift valley (Buck et al. 2006; Standish and Sims 2010).

11.4.2 Slow Ridges: The Icelandic Ridge

Although partly complicated by the activity of the mantle plume, the shallow structure of the Icelandic Ridge largely reflects the far-field processes associated with the evolution of the slow Mid-Atlantic Ridge, of which the Icelandic Ridge remains the most accessible and best-studied portion.

The Mid-Atlantic Ridge (MAR) is the most notable example of slow spreading ridge, stretching from pole to pole along the Atlantic Ocean. The MAR is frequently dissected by transform faults, especially in the equatorial region. It shares some features with ultraslow ridges, including important portions with detachment faulting exhuming lower crust to upper mantle, as between 22 and 24 °N, where ~40% of the seafloor is made of extended terrain and detachment faults. Overall, the input of magma at the spreading axis is complementary to the development of detachment faulting, but the relationship is not strong, as for example between 14 and 16 °N where detachments continued to slip despite hosting magmatic intrusions, suggesting partially concomitant activity (Cann et al. 2015; Parnell-Turner et al. 2018, and references teherein). Magmatic activity along the MAR may be also manifest in a subtler way. For example, large scale corrugations, or megamullions, of the detachments in different portions of the MAR have been interpreted to result from significant magmatic accretion below, as due to the emplacement of shallow intrusions. Therefore, an important portion of the total extension in correspondence of the detachments may be accommodated by otherwise unnoticed magmatic accretion. Magmatic accretion may also occur off-axis, explaining the much lower distribution of magmatism than that predicted by the spreading along the ridge axis alone (Tucholke et al. 2008; Searle et al. 2010). Magma chambers have been seismically imaged in different portions of the MAR, as at 23 and 37 °N, consistent with a focused melt supply at the segment centre and steep across-axis thermal gradients, indicated by the proximity with nearby active faults. These chambers commonly lie at ~3 km of depth below the sea bottom, although in some cases they may reach ~1.2 km (Calvert 1995; Singh et al. 2006; Combier et al. 2015). Events of dike injection, accompanied with seismicity and normal faulting, have been detected along the northern portion of the MAR in 2001 (Lucky Strike segment) and in 2010 (North FAMOUS and FAMOUS segments; Giusti et al. 2018).

The best-known portions of the MAR are the highly oblique-spreading Reykjanes Ridge and the emerged Icelandic Ridge, the latter being a well-documented example of the influence of a mantle plume on a rifted lithosphere. The Reykjanes Ridge is an oblique spreading ridge consisting of en-echelon magmatic systems in a dextral configuration, partly fed by the Icelandic hotspot, which induces buoyancy-driven upwelling in the mantle below and increases the

spreading rate (Searle et al. 1998; Gaherty 2001). Each of these magmatic systems constitutes a third-order oceanic segment, while multiple systems constitute second-order segments. Magma from the mantle is initially focused towards these second-order segments and then redistributed along individual magmatic systems, which may be abandoned, indicating a finite life span. The abandonment occurs within ~2 Ma, when the system has migrated sufficiently far to become isolated from its melt supply (Peirce and Sinha 2008).

Emersion of the Iceland portion of the Mid-Atlantic Ridge results from increased magma productivity due to the plume below, with low upper mantle velocities to at least 400 km depth. The plume may be confined to the upper mantle or extend down to the core-mantle boundary. As a result of the excessive production of magma, estimated as 0.2 km^3/year, and of the related underplating the crustal thickness in Iceland varies between 15 and 46 km (Sigmundsson 2006b, and references therein; Jenkins et al. 2018). Spreading between the Eurasian and North American plates along a ~N100° direction and up to 1.8 cm/year is taken up within a ~100 km wide plate boundary along two main neovolcanic zones (Fig. 11.15; Geirsson et al. 2006; Sigmundsson et al. 2020, and references therein). To the west, is the Reykjanes-Langjokull Volcanic Zone, including the obliquely spreading Reykjanes Peninsula rift to the southwest, and the Western Volcanic Zone (WVZ) to the northeast, comprising the Hengill-Langjokull systems. The WVZ has been the main locus for crustal spreading in South Iceland for the last 6–7 Ma. To the east, the neovolcanic zone comprises the Northern Volcanic Zone (NVZ), active for 6–7 Ma, to the north of the Vatnajokull icecap, and the Eastern Volcanic Zone (EVZ), active for 2–3 Ma, to the south of it. The EVZ is propagating southwards, and significant crustal spreading has only developed north of Torfajokull volcano. The EVZ and WVZ overlap in Southern Iceland, so that the spreading rate of the EVZ decreases southward, while along the WVZ it increases southwards, maintaining an overall constant total rate. The area enclosed by the EVZ and the WVZ forms the South Iceland Seismic Zone, producing

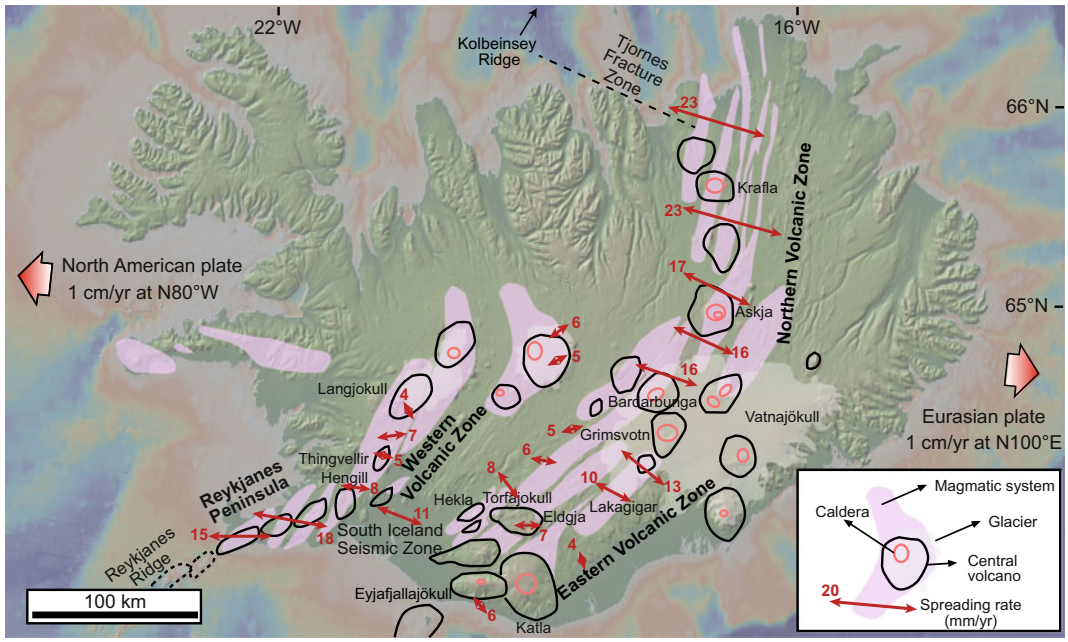

Fig. 11.15 Main tectono-magmatic features of Iceland, including the magmatic systems and the 1986–2002 GPS spreading rates (double arrows; Perlt et al. 2008). Base DEM provided by GeoMapApp

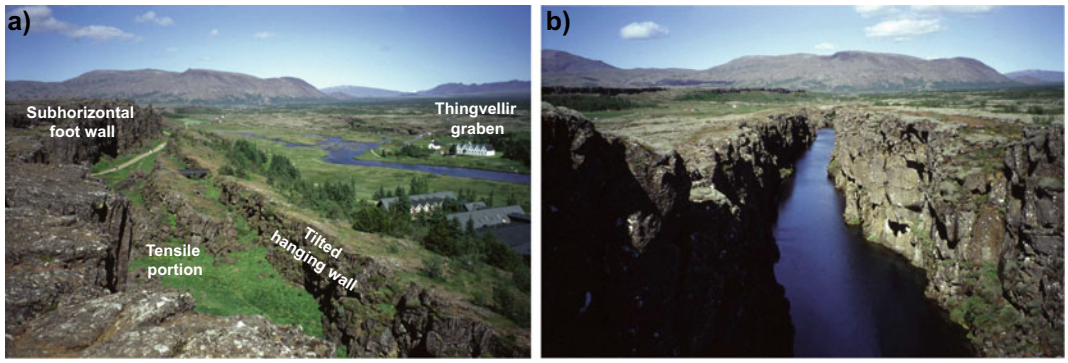

Fig. 11.16 Examples of **a** open normal fault with tilted hanging wall and **b** metre- wide extension fracture at Thingvellir, southwest Iceland

$M > 7$ earthquakes, with a tectonic frame consistent with the early stages of development of a transform-like feature (Perlt et al. 2008; Angelier et al. 2008).

Surface deformation along the active rift zone consists of extensional (tension) fractures and normal faults, commonly with a dilational component between the tilted hanging wall and the horizontal foot wall, as observed along the MER and Afar (Fig. 11.16). The normal faults may form with two main mechanisms. (a) From the coalescence of joints within the lava pile, growing into extensional fractures under a tensional σ_3 and propagating downward to become shear fractures (normal faults) at several hundreds of metres of depth: this scenario implies a regional tectonic origin for the normal faults. (b) Following the emplacement of dikes, with the normal faults propagating downward from the surface and forming graben-like structures above the dikes. Recent evidence, also from diking episodes outside Iceland, suggests that mechanism (b) is the most likely and also generally applicable to magmatic divergent plate boundaries (Gudmundsson 1992; Grant and Kattenhorn 2004; Rowland et al. 2007; Acocella and Trippanera 2016).

Volcanism focuses along the rift axis, in 40–150 km long and 5–20 km wide magmatic systems, each with a dominant volcano often with evolved composition and summit caldera. Outside the dominant volcano, eruptive fissures with monogenic cones, associated with extension fractures and normal faults, highlight the continuation of the magmatic system (Fig. 11.17; Gudmundsson 1995). The eroded Late Tertiary

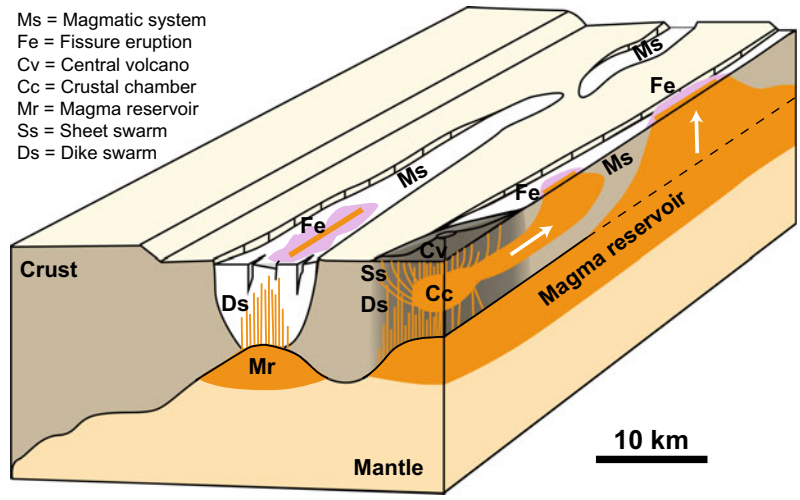

Fig. 11.17 Structure of magmatic systems along the Icelandic ridge. Fissure eruptions may be fed by the lateral propagation of dikes from a central volcano (dark area) and/or vertical propagation of dikes from the mantle below the system (white arrows; modified after Gudmundsson 1995)

and Pleistocene lava piles at the eastern and western sides of Iceland show that magmatic systems at depth consist of local sheet swarms and regional dike swarms. The sheet swarms are confined to extinct volcanoes and are usually 45°–65° inward dipping, circular to elliptical in distribution, with radius of several kilometres. Most sheet swarms are associated with plutons at 1–2 km of paleodepth. The regional dikes occur outside the eroded central volcanoes in 50 km long and 5–10 km wide swarms. These dikes are usually parallel, vertical and thicker than the sheets (see Fig. 7.4). The sheets follow the trajectories of the near-field stress around the source chambers feeding frequent, small volume proximal eruptions, whereas the regional dikes are controlled by the far-field stress, feeding larger but less frequent distal eruptions. Also, while the sheets are supplied by the shallower portion of the plumbing system, the regional dikes are supplied by the deeper portion. Magma chamber formation is facilitated by stress barriers leading to the formation of sills. The magma chamber acts like a trap for upward propagating regional dikes from mantle reservoirs and channels magma, through sheets, towards the surface (see Sect. 4.6). The eroded portions of Iceland also show that dike swarms at depths greater than ~1 km take up most of the crustal extension, with negligible contribution from normal faults. At shallower depths, the frequency of the dikes decreases, while the contribution of normal faults and, subordinately, extension fractures on extension progressively increases (Fig. 10.23; Helgason and Zentilli 1985; Gudmundsson 1986; Forslund and Gudmundsson 1991).

Within the period of geodetic measurements, most of the 35 active volcanoes in Iceland have not deformed. The deformed volcanoes inflated and deflated with rates from mm/year to cm/year (Sigmundsson et al. 2006b; Einarsson 2018). The most active and erupting Holocene volcanoes are Hekla, Katla and Grimsvotn, in the EVZ. Hekla shows the most regular behaviour, as the volume of its eruptions scales with the preceding eruptive period, producing ~1 km^3 of magma each century. Magma chambers lie at ~3 km of depth below Krafla, Katla, Askja and Grimsvotn volcanoes; other volcanoes, such as Hekla, do not have evident magma chamber shallower than 14 km depth. Although basaltic volcanism dominates, historical activity also features andesites, dacites and rhyolites. About 80% of historical eruptions occurred along EVZ. Magma productivity in the last 1100 years equals ~87 km^3 DRE, with 71 km^3 in the EVZ, with an average of 20–25 eruptions per century. Collectively, the EVZ and WVZ only erupted ~15% of total intruded volume in 1130 years (Thordarson and Larsen 2007). An overview of the tectonic and magmatic features of the main portions of the Icelandic Ridge is provided below.

The Reykjanes Peninsula consists of 5 magmatic systems in a dextral en-echelon configuration, highly oblique to the rift axis and undergoing significant left-lateral motion (1.1–1.8 cm/year). Along the margins of the magmatic systems, longer faults are subparallel to the rift axis, whereas in the centre of the system the shorter fractures strike approximately parallel to the eruptive fissures and perpendicular to the direction of minimum principal stress σ_3. The amount of geodetic extension is variable: while absent in 1993–1998, an extension of ~0.7 cm/year has been recognized between 2000 and 2006, confirming episodic rift opening. Focal mechanisms from earthquakes show a local variation of the extension direction (from N120° to N140°) along the Peninsula with regard to the regional one (N105°). In the last 4 ka, rifting episodes occurred in several portions of the Reykjanes Peninsula with average duration of ~500 years and recurrence period of ~700 years (Hreinsdottir et al. 2001; Angelier et al. 2004; Keiding et al. 2009; Saemundsson et al. 2020). To the north, the WVZ undergoes nearly orthogonal extension, alternating volcanic events and faulting on a time scale of 10^3 years, as at Thingvellir. In particular, the 40 km long and 5–7 km wide Thingvellir Graben dissects the 9000 year old pahoehoe basaltic lava flow with extension rates between 0.3 and 0.8 cm/year (Sinton et al. 2005).

In the Northern Volcanic Zone, the long-term spreading axis passes through and changes direction at the main central volcanoes, and does not follow the general direction of each fissure swarm (Drouin et al. 2017). The Krafla magmatic system is one of the most developed and active, having experienced a rifting episode between 1975 and 1984 (Fig. 11.18). In this episode, the central magma chamber fed ~20 dikes that propagated over ~80 km laterally, inducing surface fracturing and faulting with up to 2 m of vertical displacement. During the rifting sequence, magma from depths higher than 5 km accumulated in the Krafla magma chamber, at ~3 km of depth, above which deflation was observed during lateral dike injection (Bjornsson et al. 1977; Sigurdsson 1980; Arnadottir et al. 1998). Approximately 250×10^6 m^3 of basaltic lavas were erupted from eruptive fissures during the rifting episode, but a substantially larger volume, ~1 km^3, remained intruded, Maximum cumulated widening of ~9 m occurred 10–12 km north of Krafla (Fig. 11.19). Between 1992 to 1995, a subsidence of 2.4 cm/year above the Krafla magma chamber and of 0.7 cm/year along the magmatic system have been interpreted as due to cooling contraction and ductile flow of material away from the spreading axis. Similar processes have been invoked to explain the continuous deflation of the nearby Askja caldera between 1983 and 1998. The post-rifting spreading rate of the NVZ between 1987 and 1992 was higher than 3.0 cm/year and between 1993 and 2004 was 2.3 cm/year, slowing but still higher than the 1.8–2.0 cm/year predicted spreading rate, with a behaviour similar to that observed at Asal and

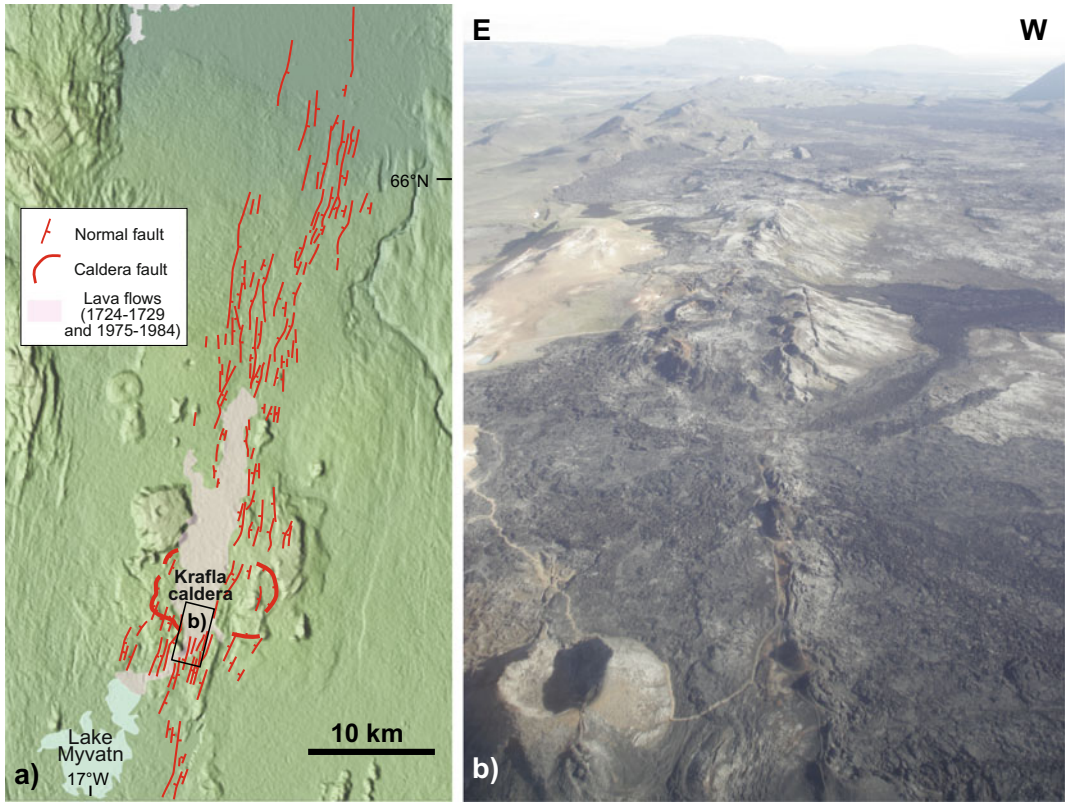

Fig. 11.18 The Krafla magmatic system, northern Iceland. **a** Overview of the magmatic system; base DEM provided by GeoMapApp. **b** View of the portion of the 1975–1984 eruptive fissure within Krafla caldera, Iceland, associated with normal faults, scoria cones and lava flows (location shown in a; photo courtesy Joel Ruch)

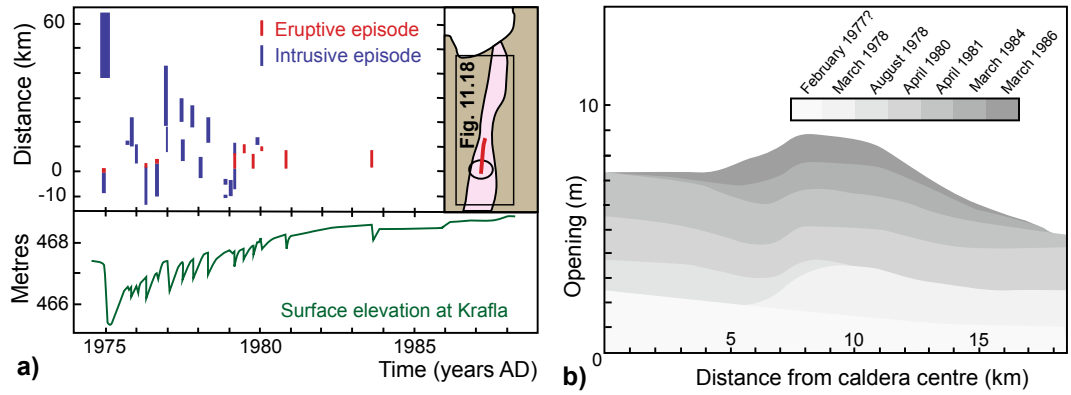

Fig. 11.19 The 1975–1984 Krafla rifting episode, Iceland. **a** Observations at Krafla between 1974 and 1989. Top: distance ranges for surface fissuring (blue) or extrusion of lava (red) measured from Krafla caldera (map, right). Thickness of the vertical lines gives duration of the activity. Bottom: changes in the elevation near the centre of inflation in the Krafla caldera; tick marks are for the beginning of each year (modified after Buck et al. 2006). **b** Opening across the Krafla fissure swarm during the rifting episode. Contributions of individual events are shown versus northward distance from Krafla caldera (modified after Sigmundsson 2006b)

Manda Hararo, in Afar (Tryggvason 1984; Sigmundsson et al. 1997; Sturkell and Sigmundsson 2000; Buck et al. 2006; Arnadottir et al. 2009). A rifting event occurred to the south, at Bardarbunga, in 2014. Here a segmented dike propagated laterally over 14 days for more than 45 km along the Bardarbunga magmatic system at a variable rate, with topography influencing the direction of propagation (Fig. 11.20; Sigmundsson et al. 2015). The strike of the dike segments varied from an initially radial direction away from the Bardarbunga caldera, towards alignment with that expected from regional stress at the distal end. Seismicity, dike opening and magma eruption focused at the distal portion, and were simultaneous with magma source deflation and slow collapse at the Bardarbunga caldera, accompanied by *M5* earthquakes. In the NVZ, rifting episodes or events appear to occur in the same magmatic system with a frequency of approximately every few hundred of years, with previous rifting sequences occurring at Krafla in 1724–1729, at Bardarbunga in 1797 and at Askja in 1874–1875. In particular, the 1875 formation of the Oskjuvatn caldera was part of a rifting episode at the Askja magmatic system that reactivated the Sveinagja Graben to the north, possibly under lateral flow of magma from the Askja reservoir, although the magma erupted along the Sveinagja Graben was different from that erupted in the caldera area and volumetric calculations do not require lateral magma propagation (Gudmundsson and Backstrom 1991; Sigmundsson 2006b; Hartley and Thordarson 2012). The EVZ has also produced several rifting episodes in historical times. Among these is the ~934 AD rifting episode at Eldgjà, feeding a nearly 70 km long eruptive fissure, and the 1783–1784 rifting episode at Lakagigar. The latter opened a 27 km long dike-fed eruptive fissure, producing one of the largest historic basaltic lava flows (nearly 15 km^3) propagating towards and activating the nearby Grimsvotn central volcano (Fig. 1.12b; Thordarson and Self 1993). Available evidence indicates that these rifting episodes are usually related to the lateral propagation of the dike(s), feeding the eruption from the magma chamber of the dominant volcano of the magmatic system. The magma feeding these fissures may rise from Moho depths within a few days (Mutch et al. 2019).

11.4.3 Fast and Ultrafast Ridges: The East Pacific Rise

Fast (spreading rate >8 to <12 cm/year) and ultrafast (>12 cm/year) oceanic ridges constitute the end-member type of divergent plate

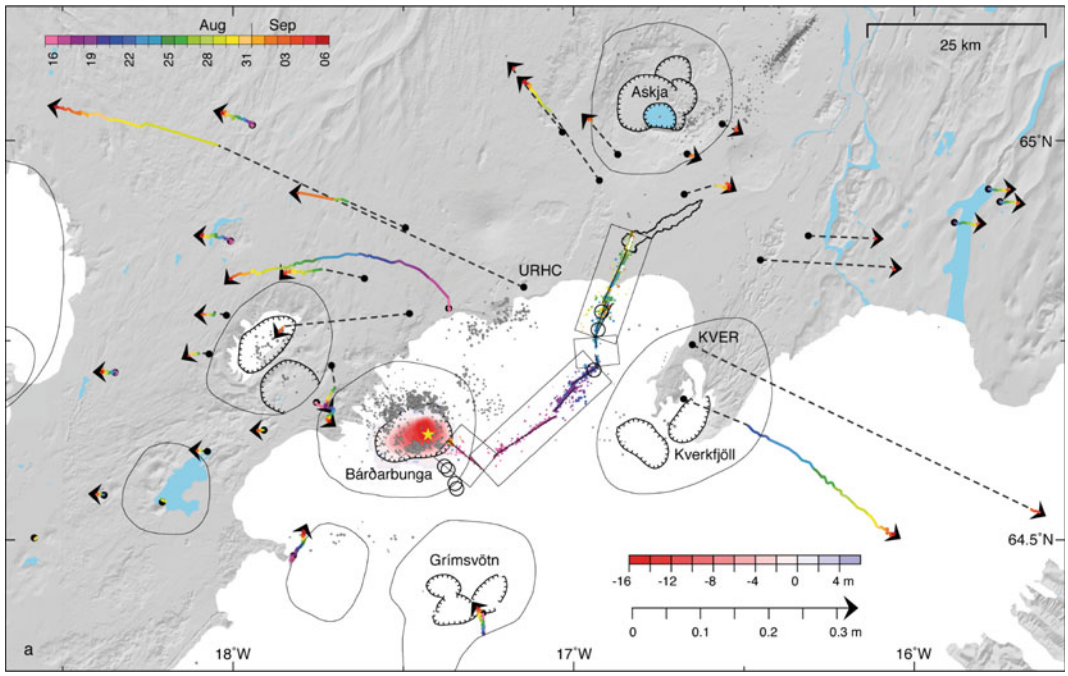

Fig. 11.20 The 2014 Bardabunga spreading event, Iceland (Sigmundsson et al. 2015). Earthquakes from 16 August to 6 September 2014 (dots) and GPS horizontal ground displacements (arrows) with central volcanoes (elliptical outlines), calderas (hatched) and northern Vatnajokull glacier (white). Epicentres and displacements are colour coded according to time of occurrence (key at top left); other single earthquake locations are in grey. Rectangles show areas characterized by dike injections and thin lines within show inferred dike segments. The red shading at Bardarbunga caldera shows subsidence up to 16 m inferred from radar profiling on 5 September. The star marks the location of the magma source inferred from modelling. Also shown are ice cauldrons formed (circles), outline of lava flow mapped from radar image on 6 September, and eruptive fissures (white). Image courtesy Freysteinn Sigmundsson

boundary. The fastest oceanic ridge, approaching a full spreading rate of 15 cm/year, is the East Pacific Rise (EPR), running from the Gulf of California to off Antarctica in the southeastern Pacific Ocean. The EPR is segmented, with the longevity of its segments increasing with their hierarchical order. While first-order volcanic segmentation remains fairly stable, the fourth-order segmentation, including the patterns of local hydrothermal activity, may undergo repeated reorganization. The EPR has prominent bathymetry, with a focused **axial rise**, or topographic high, 5–20 km wide and 200–500 m above the background slope, tapering along rift towards transform faults and overlapping spreading centres. The axial rise may be generated by the dynamic extensional stresses relieved by diffuse diking in the upper lithosphere, with dikes usually dipping away from the axis, as well as by variations in the bulk density of oceanic crust caused by magmatic differentiation, attributed to the geometry of mantle upwelling (Macdonald 1998; White et al. 2002; Toomey and Hooft 2008).

The zone of active faulting, or plate boundary zone, along a fast spreading ridge is a few tens of kilometres wide, with widespread inward and outward dipping faults. For example, along the East Pacific Rise between 8° 30′ N and 10° 00′ N, the zone of active faulting is approximately 90 km wide. Here both inward and outward dipping fault scarps increase in

height away from the ridge, reaching average heights of ~100 m at ~45 km from the ridge axis; beyond this distance, there is no significant increase in scarp height (Crowder and Macdonald 2000). Although widespread, here surface faulting accounts only for a limited portion (5–10%) of the total spreading and seems to occur mainly with minor seismicity or aseismically. The development of part of these inward and outward dipping normal faults over a zone much wider than the ridge axis results from the bending of the plate at the axial rise. Removal of the topographic effect of faulting from the original seafloor bathymetry reveals a gently inward dipping surface (towards the ridge axis), possibly resulting from subsurface magma withdrawal associated with dike injection and eruption (Carbotte et al. 2003; Shah and Buck 2003).

In the central portion of the axial rise, some parts (approximately 15–20%) of the EPR show a narrow (usually up to two kilometres wide) and deep (usually up to 100 m) **axial trough** (Fig. 11.21). The trough is commonly interpreted as the surface effect of a narrow and highly active dike intrusion zone, which produces a graben-like structure, consistently with the mechanisms discussed in Sect. 7.7. In particular, the narrower and deeper structure of the axial trough with regard to grabens formed during dike intrusions along slower divergent plate boundaries implies a very shallow emplacement for the responsible dikes, which are inferred to have a relatively high internal magma pressure, thus largely representing feeder dikes (Chadwick and Embley 1998; Fornari et al. 1998). The structure of the axial trough has been related not simply to dike emplacement, but also to the intrusive to extrusive frequencies affecting a portion of the ridge. In particular, extremely narrow axial troughs (a few tens of m wide) have been interpreted to

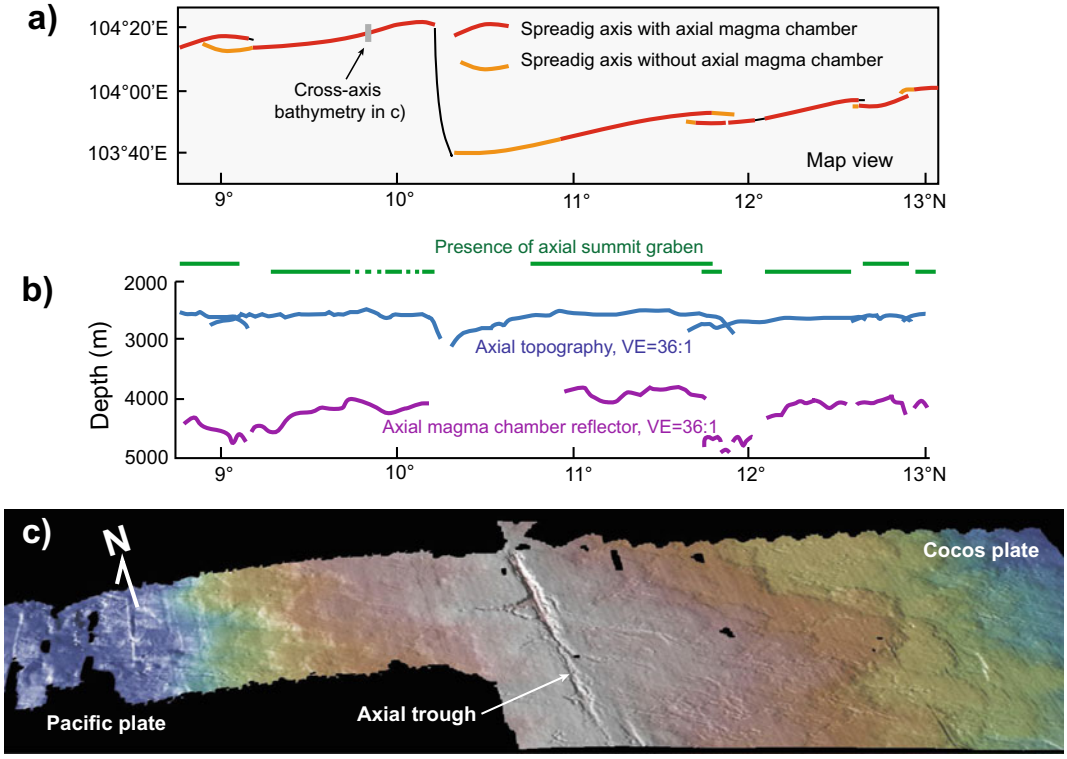

Fig. 11.21 **a** Schematic map view of portion of the fast spreading East Pacific Rise and **b** its main topographic, structural and magmatic features in section view (Macdonald and Fox 1988). **c** Oblique bathymetric view of the EPR at 9° 50′ N (location in **a**; from GeoMapApp). VE = vertical exaggeration

result from recent dike-induced volcanism, whereas the absence of axial troughs may result from a decrease in the eruptive frequency (Soule et al. 2009). Alternatively, the axial trough has been interpreted as an extremely elongated and narrow collapse caldera structure related to the waning activity of the underlying magma chamber (Lagabrielle and Cormier 1999).

Below the axial trough or, more in general, the ridge axis there may be pipe-like zones of vigorous hydrothermal activity, directly fed from underlying magma chambers and generating massive sulphide ore deposits. The seismicity associated with these zones suggests that hydrothermal circulation is strongly aligned along, and not across, the ridge axis (Tolstoy et al. 2008). Most importantly, the portion below the trough also coincides with robust and focused magma supply, through dikes, from the frequently seismically imaged shallow axial reservoirs, which commonly show a sill-like shape. In particular, along the EPR between 8° 20′ N and 10° 10′ N several sill-like magma reservoirs have been imaged at a mean depth of 1.6 km below the seafloor, with a ~6 km dominant length possibly reflecting the spacing of local sites of ascending magma from discrete melt reservoirs pooled beneath the crust. Multi-level complexes of magma lenses have been also imaged, contributing to the formation of both the upper and lower crust (as between 9° 20′ and 9° 57′ N), or resulting from the overlap of two ridge segments (as at the 9° N overlapping spreading centre; Canales et al. 2009; Arnulf et al. 2014; Marjanovic et al. 2014; Marjanovic et al. 2018). Studies based on the anisotropy of magnetic susceptibility (AMS) on samples indicate distinct compositional sources that feed melt injected into dikes with no preference for subhorizontal or subvertical magma flow, consistently with AMS data from ophiolites in Oman or Cyprus. Moreover, the well-imaged sill-like magma reservoirs between 8° 20′ N and 10° 10′ N at ~1.6 km below the seafloor form 5–15 km long segments that coincide with the fine-scale tectonic segmentation at the seafloor. Here transitions in composition, volume and morphology of erupted lavas coincide with disruptions in the lens that define magmatic systems. This suggests that eruptions at the EPR are associated with the vertical ascent of magma from lenses that are mostly physically isolated, leading to the eruption of distinct lavas at the surface that coincide with fine-scale segmentation (Fig. 11.22; Carbotte et al. 2013; Horst et al. 2014).

The mechanisms of lower-crustal accretion may vary along the EPR, as inferred between 9° 42′ and 9° 57′ N, but the volume of melt delivered to the crust appears mostly uniform. In particular, the continuous and shallow along-axis melt bodies of the EPR provide a robust magma supply, fed by narrow vertical transport down to 70 km within the mantle (Forsyth et al. 1998; Kent et al. 2000). This area is overlying a deeper vertical flow, associated with long-lived and deep-seated (down to the lower mantle) upwelling. This mantle-wide upwelling is inferred to drive horizontal components of asthenospheric flows beneath the plates that are faster than the overlying surface plates, thereby contributing to plate motions through viscous tractions in the Pacific region. Therefore, rather than being correlated to slab pull in the Circum-Pacific area, the high spreading rate of the EPR seems more related to stable mantle-scale upwelling (Gu et al. 2005; Rowley et al. 2016).

Off-axis volcanism may be present along fast spreading ridges, as from 9° 37′ to 9° 57′ N. This volcanism does not necessarily derive from a sub-axial magma body, being rather sourced directly from off-axis magma bodies with longer period of melt replenishment, lower eruption recurrence rates, and lower eruption volumes than the axial magma lens. Such off-axis magmatism may occur preferentially where pre-existing fractures inherited from offsets of the spreading axis promote melt transport from the mantle into the crust (Canales et al. 2012; Waters et al. 2013).

Seafloor spreading episodes have been also documented. In 2005–2006, a progressive build up in seismicity opened the EPR at 9° 50′ N (location in Fig. 11.22; Tolstoy et al. 2006; Dziak et al. 2009; Fundis et al. 2010; Xu et al. 2014). The resulting submarine eruptions

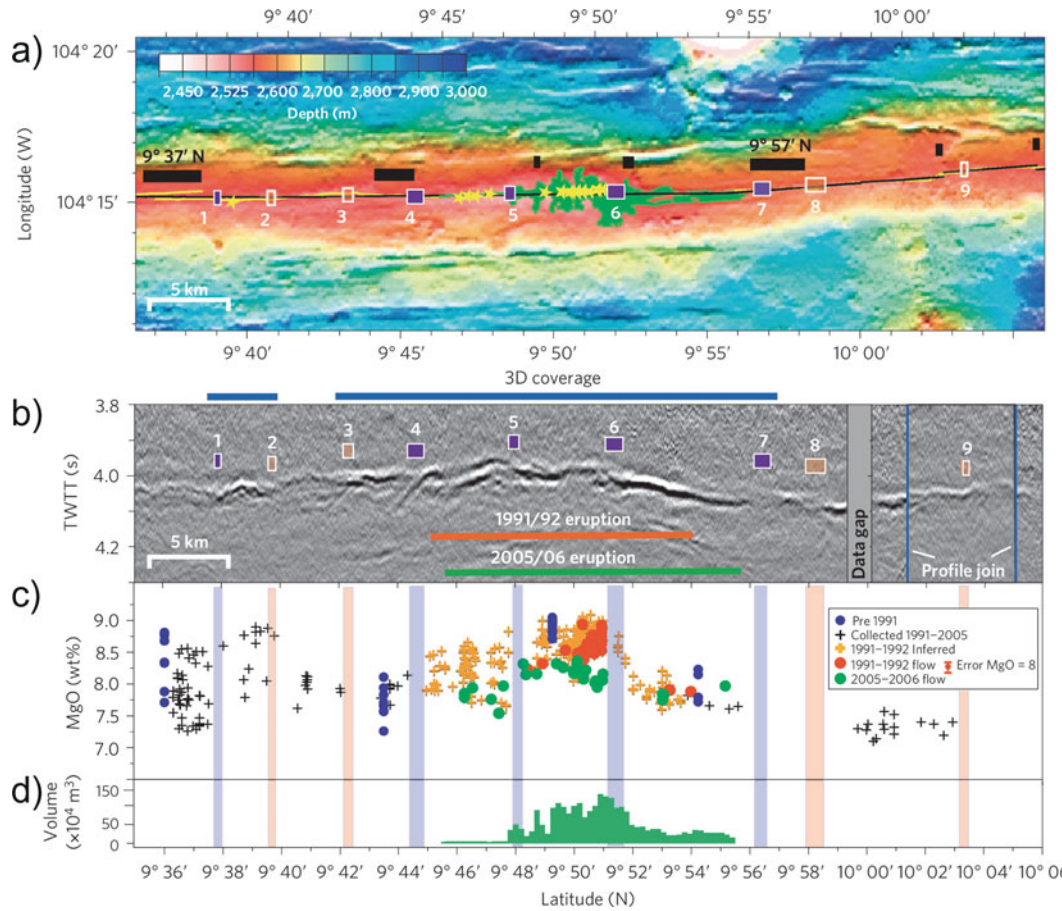

Fig. 11.22 Segmentation in seafloor structure, axial magma lens, lava geochemistry and eruption volume along the East Pacific Rise 9° 35′–10° 06′ N. **a** Bathymetry showing location of axial eruptive zone (yellow line) and composite axial seismic profile (black). Black rectangles: third- (labelled) and fourth-order tectonic discontinuities. Yellow stars: hydrothermal vents; green region: 2005–2006 lava flow. **b** Composite axial seismic reflection section showing magma lens reflection and interpreted disruptions. TWTT, two-way travel time of seismic waves. Numbered rectangles in **a**, **b** indicate magma lens disruptions identified from seismic data (purple, data from 3D seismic volume). **c** MgO composition of seafloor lavas located within 500 m of the axis colour-coded for eruption period. **d** Volume of erupted 2005–2006 lavas. Vertical bars (translucent purple and orange) mark magma lens disruptions from **a** and **b** (Carbotte et al. 2013)

activated multiple vents, with either rapid bilateral propagation of feeder dikes along the rift or near simultaneous vertical injection of melt. The stress changes due to dike intrusion along the ridge promoted normal faulting and strike-slip motion within the nearby transform zone. A total magma volume of 9–83 $\times$ 10^6 m^3 was extracted from a 5 km long section of the ridge axis, with a maximum of 71 $\times$ 10^6 m^3 left unerupted in the crust as dikes. An eruption of similar dimensions may have a frequency of years to decades to sustain the long-term average seafloor spreading rate at this location. The pre-eruptive increase in seismicity has been interpreted as mainly resulting from tectonic stress building up to a critical level along most of the ridge segment, rather than magma overpressure in the underlying magma lenses (Tan et al. 2016). This implies that, if plate pull may dominate at magmatically robust fast-spreading ridges, it could also dominate at

intermediate and slow spreading ridges, with relatively lower magma supplies. From December 2009 to October 2011, the same area underwent up to 12 cm of inflation, induced by a point source along the ridge axis at a depth of 2.7 km, possibly recharged from a deeper source (Nooner et al. 2014).

11.5 A General Model for Divergent Plate Boundaries

This chapter has highlighted an intensification in the importance of magmatic processes along divergent plate boundaries with progressively higher extension rates. In immature continental rifts, as the non-volcanic portions of the EARS and the southern MER, as well as in non-magmatic portions of ultraslow oceanic ridges, regional extensional tectonics is the main mechanism responsible for divergence. Here the role of any magmatic activity on rifting appears subordinate, at least at upper crustal levels. Prolonged regional extension or, more effectively, increased extension rates may enhance decompression melting and the rise and shallow intrusion of magma (Fig. 11.23; Ebinger and Hayward 1996). This promotes a mature and magmatically active continental rift, such as the northern MER, where magma assists rifting. This condition eventually evolves into a transitional rift supported by an increased magmatic budget partially replacing the continental crust, as observed in Afar. Further extension leads to focused and magma-dominated rifting on oceanic crust, with variations in the continuity, structure, shape and stability of the active spreading zone mainly depending on the spreading rate.

In this ideal evolution, the contribution of magmatic activity on rifting manifests at progressively shallower levels, first intruding dikes mainly within the lower crust (continental rifts) and subsequently intruding the upper crust with sills generating magma chambers and propagating dikes feeding longer magmatic systems (transitional and oceanic rifts). The effectiveness of magmatic activity in separating the plates on any crustal domain is supported by the above-mentioned recent dike-induced spreading episodes and events in the Afar region, the Aden

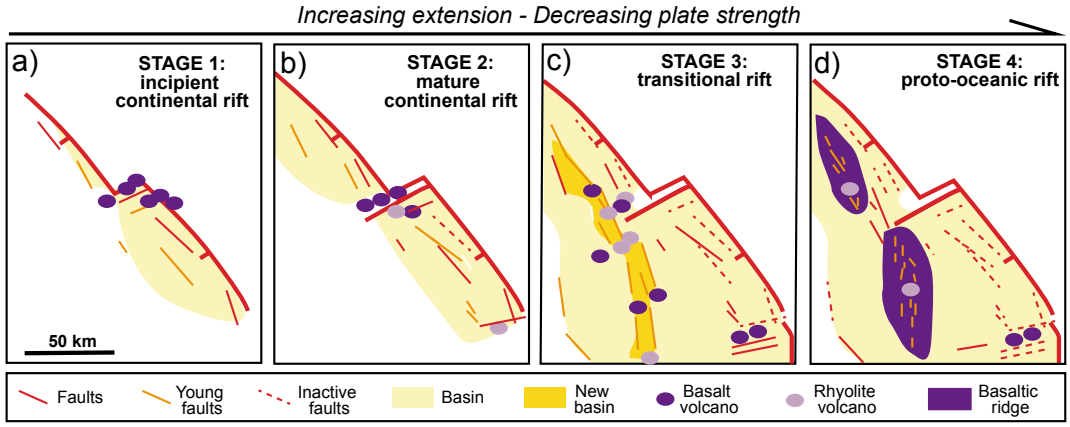

Fig. 11.23 Schematic variations in rift architecture and volcanism as the spreading rate increases in a continental to transitional rift (modified after Ebinger and Hayward 1996). **a** Immature continental rifts: faults and basins, predominantly asymmetric, within relatively strong lithosphere and basaltic volcanism along border faults. **b** Mature continental rifts: as extension increases, the rift becomes more symmetric and eruptive centres (including rhyolitic ones) move into the rift valley. **c** Rift on transitional crust: increasing the extension induces a broader rift zone, with shorter faults and an inner rift valley, with bimodal (basaltic and rhyolitic) volcanism. **d** Proto-oceanic rifts: continued extension may develop basaltic ridges along the rift axis

and Red Sea Rifts, the MAR, Iceland and the East Pacific Rise (Table 11.1). Studies on the rifting episodes in Iceland and Afar (Krafla and Manda Hararo episodes) highlight that the initial and largest dike intrusion within each episode was followed by a series of smaller intrusions. All these dike intrusions obey scaling relationships similar to earthquakes, with the dimensions of the dikes following a power law behaviour analogous to the Gutenberg-Richter relation (Passarelli et al. 2014). Each of these episodes represents the culmination of a **rifting cycle**, where the diking events (co-rifting phase) open the plate boundary by several metres, releasing the stresses built up through continuous longer-term stretching (inter-rifting phase). The co-rifting displacement decreases with across-strike distance from the rift axis, where the opening due to the intrusion superimposes over the steady state tectonic rate. For a few decades after the rifting event (post-rifting phase), the spreading rate along the rifted portion of the plate boundary

Table 11.1 Comparison among major instrumentally-detected diking episodes or events along continental and oceanic divergent plate boundaries, including the magnitude range of associated earthquakes (*M*), the seismic (SM) and geodetic (GM) moment, their ratio (SM/GM; representing the seismic component associated with the total displacement) and the volume of involved magma

Area	Period	*M*	Seism. Mom. (*SM*) (10^{17} Nm)	Geod. Mom. (*GM*) (10^{17} Nm)	*SM/GM* (%)	Volume (km^3)	Ref.
Krafla	1975–1984	6.3	58	440–900	8.6	1.6	a
Dallol	Oct–Nov 2004	2.6–5.5	2.28	22.0	10.4	0.058	b
EPR (9° 50′ N)	2005–2006	~2–3.5				~0.12	c, d
Dabbahu	Sep 2005	1.8–5.5	25–34	800–896	3.1–3.8	1.8–2.5	b, e, f
	Jun 2006	2.5–4.7	1.80	54.4	3.3	0.120	g
	Jul 2006	2–3	0.02	32.4	0.1	0.042	g
	Sep 2006	2.6–3.4		32.0	0.1	0.088	b
	Aug 2007	<3	0.01	24.1	0.0	0.048	g
	Nov 2007	2.9–4.5	1.03	60.1	1.7	0.15	g
	Mar–Apr 2008	<3.0	16	37.2	0.4	0.088	g
	Jul 2008	<3	0.08	32.1	0.2	0.066	g
	Oct 2008	1.8–4.6	1.78	78.8	2.3	0.17	g
	Feb 2009	2–3.5	0.27	30.2	0.9	0.077	g
	Jun 2009	<4	0.01	18.1	0.1	0.046	g
Lake Natron	Jul–Aug 2007	3–5.9	14.00	40.0	35.0	0.09	h
Harrat Lunayyir	Apr–Jun 2009	3–5.4	2.79	44.1	6.3	0.13	i
Bardarbunga	Aug-Dec 2014	≤5.7	51 (*); 0.2 (**)	190	26.9	~0.5	k, l, m

Ref references. [a]Hollingsworth et al. (2013); [b]Nobile et al. (2012), and references therein; [c]Dziak et al. (2009); [d]Xu et al. (2014); [e]Wright et al. (2006); [f]Grandin et al. (2009); [g]Belachew et al. (2011); [h]Calais et al. (2008); [i]Pallister et al. (2010); [k]Icelandic Met Office; [l]Kristin Vogfjord and Simone Cesca (personal communications); [m]Andy Hooper (personal communication); * at the caldera; ** along the dike

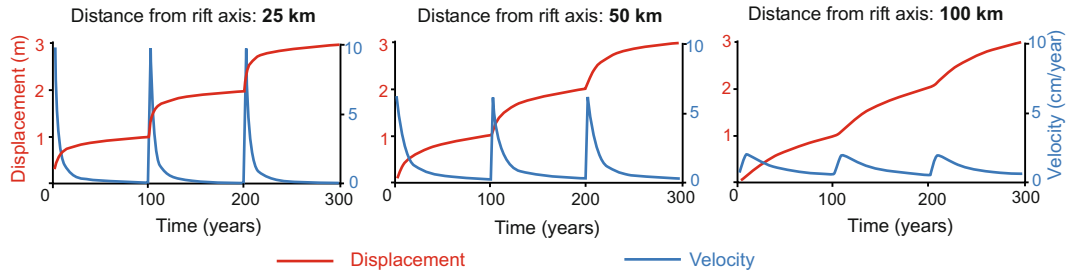

Fig. 11.24 Near- and far-field kinematic behaviours of a spreading plate boundary. Displacement (red lines) and velocity (blue lines) versus time, shown for different distances from the boundary axis: **a** 25 km; **b** 50 km; **c** 100 km (modified after Sigmundsson 2006b)

remains higher than the predicted one, as repeatedly observed in Afar and Iceland (Fig. 11.24). Oblique spreading may increase the time recurrence between major rifting episodes, as a consequence of a decrease in the amount of extension and increase in the shear component. Such behaviour is observed in the Reykjanes Peninsula (Iceland), where magma supply is limited and widening of the plate boundary may need up to a thousand years (Sigmundsson 2006b; Saemundsson et al. 2020). These diking episodes imply a subordinate role of regional tectonics in extending the crust, supported by the theoretical evidence that the stress required to tectonically separate the lithosphere by means of normal faulting (in the order of ~65 MPa) is higher than that required to magmatically rift it by means of dikes (that is less than 10 MPa) (Fig. 11.25; Buck 2006). Nevertheless, the 2005–2006 rifting episode at 9° 50′ N along the East Pacific Rise, likely triggered by the build up in the tectonic stress, implies that magma may be assisted by regional tectonics even in the most favourable conditions for its propagation, that is in an ultrafast-spreading ridge (Tan et al. 2016). This suggests that, while the increase of the spreading rate increases the importance of magmatic activity in promoting rifting, regional tectonics may play a direct role also at the upper end of the spectrum, under the fastest spreading rates.

In this context, regional tectonic extension mainly, but not exclusively, operates on the longer-term and at the wider scale, especially imposing a stable stress field that relaxes the transient lateral compression induced by the intrusion of the dike(s), thus allowing the emplacement of further dikes. In fact, the emplacement of a dike induces at its sides a temporary increase in the rift-perpendicular horizontal component, which may pass from the minimum principal stress σ_3 that promoted dike injection to the intermediate principal stress σ_2

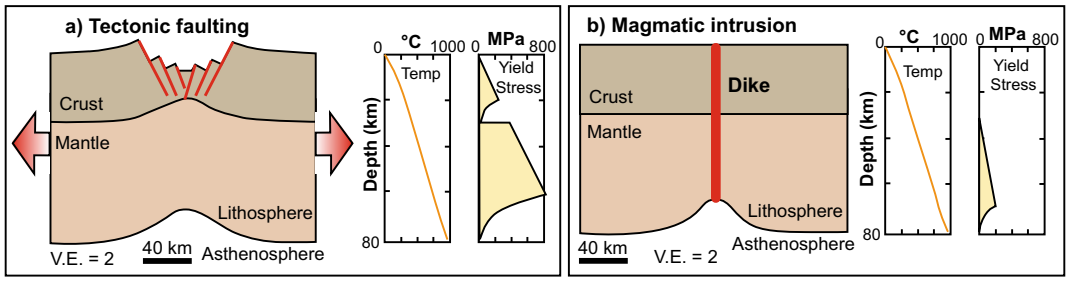

Fig. 11.25 Extension of normal thickness continental lithosphere through regional tectonic faulting (**a**) and magmatic intrusions (**b**). Note the large difference in the yield stress, or the stress difference needed to get extensional separation of two lithospheric blocks, in the two cases (modified after Buck 2006). V.E. = vertical exaggeration

and even to the maximum principal stress σ_1. Although transient, a horizontal σ_1 perpendicular to the rift may favour sill intrusion, encouraging shallow magma accumulation, until the regional stress relieves the dike-induced compression and the regional σ_3 replaces the σ_1, re-promoting dike emplacement. The repetition of this cycle, where diking episodes (controlled by the horizontal minimum principal stress σ_3) alternate to reservoir growth (controlled by the horizontal maximum principal stress σ_1), results in a feedback encouraging episodic shallow magma rise and emplacement.

Dike-fed **magmatic systems** are the fundamental unit responsible for rifting, independently of the nature of the crust (Gudmundsson 1995; Ebinger and Casey 2001). These systems may be sporadically present in immature continental rifts characterized by slow spreading rate and incipient volcanic activity, as the western branch of the EARS, or in ultraslow spreading ridges. Here magmatic systems appear as a local alternative, with limited lateral extent, complementary to the upper crustal extension resulting from regional tectonic faulting, which may manifest through normal faults bordering half-grabens (in immature continental rifts) or low-angle detachments (in ultraslow ridges). Conversely, magmatic systems are ubiquitous in divergent plate boundaries characterized by predominant magmatic activity, where they display distinctive geometric features. Along the MER, Afar, Iceland and the EPR, the larger the spreading rate, the more elongated and narrower, with lower aspect ratio A_r (where A_r = width w/length L) is the magmatic system (Fig. 11.26; Acocella 2014). This indicates that higher spreading rates are related to longer magmatic systems, where dike propagation is promoted by a weaker σ_3 and thus a higher deviatoric stress. These dikes typically feed monogenic mafic volcanism, whereas the dominant polygenic volcano of the magmatic system may erupt also felsic magma. In particular, felsic magma predominates on thicker continental crust, whereas mafic magma predominates on thinner oceanic crust. The ratio of polygenic to monogenic volcanism in a magmatic system appears also controlled by the

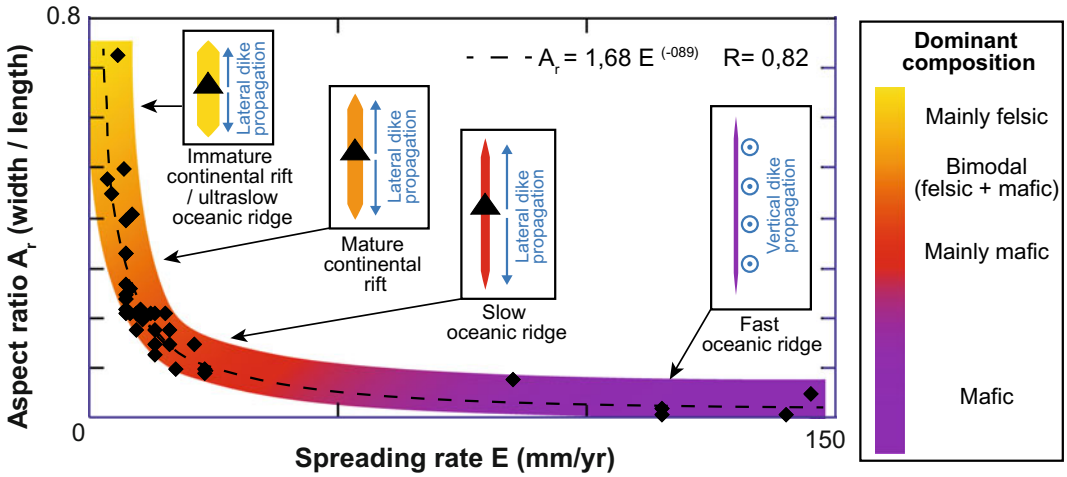

Fig. 11.26 Summary of the main features of magmatic systems along divergent plate boundaries. There is an inverse and non-linear proportion between the spreading rate of the plate boundary and the aspect ratio A_r (width/length) of the magmatic systems in immature continental rifts (and ultraslow oceanic ridges), mature continental rifts, slow oceanic ridges and fast and ultrafast oceanic ridges. Increasing the spreading rate develops progressively longer and narrower magmatic systems, also decreasing the felsic component. Insets show schematic map views of magmatic systems with different aspect ratio, also including deeper magma distribution (in blue): black triangles indicate dominant polygenic volcanoes, whereas monogenic volcanoes are not shown for simplicity. In magmatic systems with dominant polygenic volcano, the volcano magma chamber favours lateral dike propagation (blue arrows); in magmatic systems without dominant polygenic volcano (in fast oceanic ridges), the more continuous magma distribution encourages vertical dike propagation (blue circles with dots; modified after Acocella 2014)

spreading rate: polygenic volcanoes are more common in slower spreading settings and monogenic volcanoes in faster spreading settings, with higher differential stress $\Delta\sigma = \sigma_1 - \sigma_3$ and higher magmatic output (see Sect. 10.6; Takada 1994). This different distribution of volcanoes has also implications for the mode of delivery of magma along the magmatic system. In fact, in a magmatic system with dominant polygenic volcano the latter mainly feeds the monogenic fissures through laterally propagating dikes from the base of its magma chamber, as proposed for Krafla (in 1975–1984), Dabbahu (in 2005–2010) and Bardarbunga (in 2014). Where the dominant polygenic volcano is absent, as at fast spreading oceanic ridges, available evidence suggests a mainly vertical propagation of the dikes promoting rifting (Wright et al. 2012; Carbotte et al. 2013). This different mode of magma propagation derives from the different along-rift extent of the magma chamber feeding the dikes. This is more continuous in fast spreading ridges, enhancing vertical dike propagation, and of more limited extent below the polygenic volcano of slow spreading systems, where lateral dike propagation favours rifting.

The architecture of a magmatic system, in terms of aspect ratio, magma distribution, composition and delivery, is thus diagnostic to evaluate the role of magmatism on rifting along divergent plate boundaries. Magmatic systems are indeed the primary product of a divergent plate boundary defined by a given spreading rate, providing a convenient framework to evaluate its tectonic and magmatic maturity.

11.6 Summary

Divergent plate boundaries are found on continental, transitional and, mostly, oceanic crust. Regional examples show that, where magmatism is limited or absent, plate divergence occurs mainly by normal faulting, forming half-grabens or detachments, as at immature continental rifts (southern portion and western branch of the EARS) and ultraslow spreading ridges, respectively. Increasing the extension rate leads to a progressively more important and shallower magmatic contribution in rifting. This is observed in mature continental rifts (northern MER) and, especially, in transitional (Afar) and oceanic (both slow and fast) ridges, where magmatic activity via diking becomes most effective in spreading the plates. In these rifts activity focuses in magmatic systems, whose architecture, summarized by their aspect ratio, provides a framework to relate the tectonic and magmatic maturity of a divergent plate boundary, in terms of magma distribution, composition and delivery, to its spreading rate. In this frame, the laterally propagating dikes, mainly associated with the limited extent of magma chambers in slow spreading boundaries, complement the vertically propagating dikes associated with along-rift more continuous magma chambers in fast spreading boundaries.

11.7 Main Symbols Used

A_r	Aspect ratio of magmatic system
L	Length of magmatic system
M	Magnitude
w	Width of magmatic system
$\Delta\sigma$	Differential stress
σ_1	Maximum principal stress
σ_2	Intermediate principal stress
σ_3	Minimum principal stress

References

Acocella V, Trippanera D (2016) How diking affects the tectono-magmatic evolution of slow spreading plate boundaries: overview and model. Geosphere 12:1–17

Acocella V (2010) Coupling volcanism and tectonics along divergent boundaries: collapsed rifts from Central Afar, Ethiopia. Geol Soc Am Bull 122:1717–1728

Acocella V, Abebe B, Korme T (2011) Holocene opening directions along the axes of Red Sea (Afar) and Main Ethiopian rifts: an overview. In: Beccaluva L, Bianchini G, Wilson M (eds) Volcanism and evolution of the African lithosphere. Geological Society of America Special Paper, vol 478, pp 25–35

Acocella V (2014) Structural control on magmatism along divergent and convergent plate boundaries: overview, model, problems. Earth-Sci Rev 136:226–288

Agostini A, Bonini M, Corti G, Sani F, Mazzarini F (2011) Fault architecture in the main Ethiopian Rift and comparison with experimental models: implications for rift evolution and Nubia-Somalia kinematics. Earth Planet Sci Lett 301:479–492

Ahmed A, Doubrè C, Leroy S, Kassim M, Keir D, Abayazid A et al (2016) Seafloor spreading event in western Gulf of Aden during the November 2010–March 2011 period captured by regional seismic networks: evidence for diking events and interactions with a nascent transform zone. Geophys J Int 205:1244–1266

Almalki KA, Betts PG, Ailleres L (2015) The red sea—50 years of geological and geophysical research. Earth Sci Rev 147:109–140

Amelung F, Jonsson S, Zebker H, Segall P (2000) Widespread uplift and 'trapdoor' faulting on Galapagos volcanoes observed with radar interferometry. Nature 407:993–996

Angelier J, Slunga R, Bergerat F, Stefansson R, Homberg C (2004) Perturbations of stress and oceanic rift extension across transform faults shown by earthquake focal mechanisms in Iceland. Earth Planet Sci Lett 219:271–284

Angelier J, Bergerat F, Stefansson R, Bellou M (2008) Seismotectonics of a newly formed transform zone near a hotspot: earthquake mechanisms and regional stress in the South Iceland Seismic Zone. Tectonophysics 447:95–116

Arnadottir T, Sigmundsson F, Delaney PT (1998) Sources of crustal deformation associated with the Krafla, Iceland, eruption of September 1984. Geophys Res Lett 25:1043–1046

Arnadottir T, Lund B, Jiang W, Geirsson H, Bjornsson H, Einarsson P et al (2009) Glacial rebound and plate spreading: results from the first countrywide GPS observations in Iceland. Geophys J Int 177:691–716

Arnulf AF, Singh SC, Pye JW (2014) Seismic evidence of a complex multi-lens melt reservoir beneath the 9° N overlapping spreading center at the East Pacific Rise. Geophys Res Lett 41:6109–6115

Ayele A, Keir D, Ebinger CJ, Wright TJ, Stuart GW, Buck WR et al (2009) The September 2005 mega-dike emplacement in the Manda-Hararo (Afar) nascent oceanic rift. Geophys Res Lett 36:L20306. https://doi.org/10.1029/2009GL039605

Barberi F, Varet J (1970) The Erta Ale Volcanic Range (Danakil depression, northern Afar, Ethiopia). Bull Volcanologique 34:848–917

Barberi F, Varet J (1977) Volcanism of Afar: small-scale plate tectonics implications. Geol Soc Am Bull 88:1251–1266

Bastow ID, Nyblade AA, Stuart GW, Rooney TO, Benoit MH (2008) Upper mantle seismic structure beneath the Ethiopian hot spot: rifting at the edge of the African low-velocity anomaly. Geochem Geophys Geosyst 9:Q12022. https://doi.org/10.1029/2008GC002107

Bastow ID, Keir D (2011) The protracted development of the continent–ocean transition in Afar. Nat Geosci 4:248–250

Bastow ID, Booth AD, Corti G, Keir D, Magee C, Jackson CAL et al (2018) The development of late-stage continental breakup: seismic reflection and borehole evidence from the Danakil Depression, Ethiopia. Tectonics 37:2848–2862

Belachew M, Ebinger C, Coté D, Keir D, Rowland JV, Hammond JOS et al (2011) Comparison of dike intrusions in an incipient seafloor-spreading segment in Afar, Ethiopia: Seismicity perspectives. J Geophys Res 116:B06405. https://doi.org/10.1029/2010JB007908

Benoit MH, Nyblade AA, VanDecar JC (2006) Upper mantle P-wave speed variations beneath Ethiopia and the origin of the Afar hotspot. Geology 34:329–332

Biggs J, Bastow ID, Keir D, Lewi E (2011) Pulses of deformation reveal frequently recurring shallow magmatic activity beneath the Main Ethiopian Rift. Geochem Geophys Geosyst 12:Q0AB10. https://doi.org/10.1029/2011GC003662

Bilham R, Bendick R, Larson K, Mohr P, Braun J, Tesfaye S et al (1999) Secular and tidal strain across the main Ethiopian Rift. Geophys Res Lett 26:2789–2792

Birhanu Y, Bendick R, Fisseha S, Lewi E, Floyd M, King R et al (2016) GPS constraints on broad scale extension in the Ethiopian Highlands and Main Ethiopian Rift. Geophys Res Lett 43:6844–6851

Bjornsson A, Saemnundsson K, Einarsson P, Tryggvason E, Gronvald K (1977) Current rifting episode in North Iceland. Nature 266:318–323

Bonatti E (1985) Punctiform initiation of seafloor spreading in the Red Sea during transition from a continental to an oceanic rift. Nature 316:33–37

Bosworth W, Burke K, Strecker M (2003) Effect of stress fields on magma chamber stability and the formation of collapse calderas. Tectonics 22:1042. https://doi.org/10.1029/2002TC001369

Bosworth W, Huchon P, McClay K (2006) The Red Sea and Gulf of Aden Basins. J Afr Earth Sc 43:334–378

Buck WR (2006) The role of magma in the development of the Afro-Arabian Rift System. In Yirgu G, Ebinger CJ, Maguire PKH eds The Afar Volcanic Province within the East African Rift System. Journ Geol Soc London Sp Pub 259:43–54

Buck RW, Einarsson P, Brandsdottir B (2006) Tectonic stress and magma chamber size as controls on dike propagation: constraints from the 1975–1984 Krafla rifting episode. J Geophys Res 111:B12404. https://doi.org/10.1029/2005JB003879

Buck RW (2013) Magma for 50,000 years. Nat Geosci 6:811–812

Calais E, d'Oreye N, Albaric J, Deschamps A, Delvaux D, Deverchere J et al (2008) Strain accommodation by dyking in a youthful continental rift, East Africa. Nature 456:783–787

Calvert AJ (1995) Seismic evidence for a magma chamber beneath the slow-spreading Mid-Atlantic ridge. Nature 377:410–413

Canales JP, Nedimovic MR, Kent GM, Carbotte SM, Detrick RS (2009) Seismic reflection images of a near-axis melt sill within the lower crust at the Juan de Fuca ridge. Nature 460:89–94

Canales P, Carton H, Carbotte SM, Mutter JC, Nedomovic NR, Xu M et al (2012) Network of off-axis melt bodies at the East Pacific Rise. Nat Geosci 5:279–282

Cann JR, Smith DK, Escartin J, Schouten H (2015) Tectonic evolution of 200 km of Mid-Atlantic Ridge over 10 million years: interplay of volcanism and faulting. Geochem Geophys Geosyst 16:2303–2321

Cannat M, Sauter D, Lavier L, Bickert M, Momoh E, Leroy S (2019) On spreading modes and magma supply at slow and ultraslow mid-ocean ridges. Earth Planet Sci Lett 519:223–233

Carbotte SM, Tuyan WBF, Jin W, Cormier MH, Bergmanis E, Sinton J et al (2003) Magmatic subsidence of the East Pacific Rise (EPR) at 18°14'S revealed through fault restoration of ridge crest bathymetry. Geochem Geophys Geosyst 4:1008. https://doi.org/10.1029/2002GC000337

Carbotte SM, Marjanovic M, Carton H, Mutter JC, Canales JP, Nedimovic MR et al (2013) Fine-scale segmentation of the crustal magma reservoir beneath the East Pacific Rise. Nat Geosci 6:866–870

Chadwick WW, Embley RW (1998) Graben formation associated with recent dike intrusions and volcanic eruptions on the mid-ocean ridge. J Geophys Res 103:9807–9825

Chambers EL, Harmon N, Keir D, Rychert CA (2019) Using ambient noise to image the northern East African Rift. Geochem Geophys Geosyst 20:2091–2109

Chang SJ, van der Lee S (2011) Mantle plumes and associated flow beneath Arabia and East Africa. Earth Planet Sci Lett 302:448–545

Cochran JR (1983) Model for development of the Red Sea. Am Assoc Pet Geol Bull 67:41–69

Combier V, Seher T, Singh SC, Crawford WC, Cannat M, Escartín J et al (2015) Three-dimensional geometry of axial magma chamber roof and faults at Lucky Strike volcano on the Mid-Atlantic Ridge. J Geophys Res 120:5379–5400

Corti G, van Wijk J, Cloething S, Morley CK (2007) Tectonic inheritance and continental rift architecture: numerical and analogue models of the East African Rift system. Tectonics 26:TC6006. https://doi.org/10.1029/2006TC002086

Corti G (2009) Continental rift evolution: from rift initiation to incipient break-up in the Main Ethiopian Rift, East Africa. Earth Sci Rev 96:1–53

Corti G, Agostini A, Keir D, van Wijk V, Bastow ID, Ranalli G (2015) Magma-induced axial subsidence during final-stage rifting: implications for the development of seaward-dipping reflectors. Geosphere 11:563–571

Craig T, Jackson J, Priestley K, McKenzie D (2011) Earthquake distribution patterns in Africa: their relationship to variations in lithospheric and geological structure, and their rheological implications. Geophys J Int 185:403–434

Crowder LK, Macdonald KC (2000) New constraints on the width of the zone of active faulting on the East Pacific Rise 8°30'N–10°00'N from Sea Beam Bathymetry and SeaMARC II Side-scan Sonar. Mar Geophys Res 21:513–527

Desissa M, Johnson NE, Whaler KA, Hautot S, Fisseha S, Dawes GJK (2013) A mantle magma reservoir beneath an incipient mid-ocean ridge in Afar, Ethiopia. Nat Geosci 6:861–865

Deville E, Marsset T, Courgeon S, Jatiault R, Ponte J-P, Thereau E et al (2018) Active fault system across the oceanic lithosphere of the Mozambique Channel: implications for the Nubia-Somalia southern plate boundary. Earth Planet Sci Lett 502:210–220

Dick HJB, Lin J, Schouten H (2003) An ultraslow-spreading class of ocean ridge. Nature 426:405–412

Doubre C, Manighetti I, Dorbath L, Dorbath C, Bertil D, Delmond JC (2007) Crustal structure and magmato-tectonic processes in an active rift (Asal-Ghoubbet, Afar, East Africa): 2. Insights from the 23-year recording of seismicity since the last rifting event. J Geophys Res 112:B05406. https://doi.org/10.1029/2006JB004333

Doubre C, Deprez A, Masson F, Socquet A, Lewi E, Grandin R (2017) Current deformation in Central Afar and triple junction kinematics deduced from GPS and InSAR measurements. Geophys J Int 208:936–953

Drouin V, Sigmundsson F, Ofeigsson BG, Hreinsdottir S, Sturkell E, Einarsson P (2017) Deformation in the Northern Volcanic Zone of Iceland 2008–2014: An interplay of tectonic, magmatic, and glacial isostatic deformation. J Geophys Res 122:3158–3178

Dugda M, Nyblade AA, Julia J, Langston CA, Ammon CJ, Simiyu S (2005) Crustal structure in Ethiopia and Kenya from receiver function analysis: implications for rift development in eastern Africa. J Geophys Res 110:B01303. https://doi.org/10.1029/2004JB003065

Dziak RP, Bohnenstiehl DR, Matsumoto H, Fowler MJ, Haxel JH, Tolstoy M et al (2009) January 2006 seafloor spreading event at 9°50'N, East Pacific Rise: ridge dike intrusion and transform fault interactions from regional hydroacoustic data. Geochem Geophys Geosyst 10. https://doi.org/10.1029/2009GC002388

Eagles G, Gloaguen R, Ebinger C (2002) Kinematics of the Danakil microplate. Earth Planet Sci Lett 203:607–620

Ebinger CJ, Crow MJ, Rosendahl BR, Livingstone DA, LeFournier J (1984) Structural evolution of Lake Malawi, Africa. Nature 308:627–629

Ebinger CJ (1989a) Tectonic development of the western branch of the East African Rift System. Geol Soc Am Bull 101:885–903

Ebinger CJ (1989b) Geometric and kinematic development of border faults and accommodation zones, Kivu-Rusizi Rift, Africa. Tectonics 8:117–133

Ebinger CJ, Deino AL, Drake RE, Tesha AL (1989) Chronology of volcanism and rift basin propagation: Rungwe Volcanic Province, East Africa. J Geophys Res 94:15785–15803

Ebinger CJ, Hayward NJ (1996) Soft plates and hot spots: views from Afar. J Geophys Res 101:21859–21876
Ebinger CJ, Sleep NH (1998) Cenozoic magmatism throughout east Africa resulting from impact of a single plume. Nature 395:788–791
Ebinger CJ, Casey M (2001) Continental breakup in magmatic provinces: an Ethiopian example. Geology 29:527–530
Ebinger C, Ayele A, Keir D, Rowland J, Yirgu G, Wright T et al (2010) Length and timescales of rift faulting and magma intrusion: the Afar rifting cycle from 2005 to present. Ann Rev Earth Planet Sci 38:439–466
Ebinger CJ, Keir D, Bastow ID, Whaler K, Hammond JOS, Ayele A et al (2017) Crustal structure of active deformation zones in Africa: implications for global crustal processes. Tectonics 36:3298–3332
Einarsson P (2018) Short-term seismic precursors to icelandic Eruptions 1973–2014. Front Earth Sci 6:45. https://doi.org/10.3389/feart.2018.00045
Eyles JHW, Illsley-Kemp F, Keir D, Ruch J, Jónsson S (2018) Seismicity associated with the formation of a New Island in the Southern Red Sea. Front Earth Sci 6:141. https://doi.org/10.3389/feart.2018.00141
Fornari DJ, Haymon RM, Pefit MR, Gregg TKP, Edwards MH (1998) Axial summit trough of the East Pacific Rise 9°–10°N: geological characteristics and evolution of the axial zone on fast spreading mid-ocean ridges. J Geophys Res 103:9827–9855
Forslund T, Gudmundsson A (1991) Crustal spreading due to dike and faults in southwest Iceland. J Struct Geol 13:443–457
Forsyth DW, Webb SC, Dorman LM, Shen Y (1998) Phase velocities of Rayleigh waves on the MELT experiment on the East Pacific Rise. Science 280:1235–1238
Franke D, Jokat W, Ladage S, Stollhofen H, Klimke J, Lutz R et al (2015) The offshore East African Rift System: structural framework at the toe of a juvenile rift. Tectonics 34:2086–2104
Fundis AT, Soule SA, Fornari DJ, Perfit MR (2010) Paving the seafloor: volcanic emplacement processes during the 2005-2006 eruptions at the fast spreading East Pacific Rise, 9°50′N. Geochem Geophys Geosyst 11:Q08024. https://doi.org/10.1029/2010GC003058
Furman T, Nelson WR, Elkins-Tanton LT (2016) Evolution of the East African rift: drip magmatism, lithospheric thinning and mafic volcanism. Geochim Cosmochim Acta 185:418–434
Gaherty JB (2001) Seismic evidence for hotspot-induced buoyant flow beneath the Reykjanes Ridge. Science 293:1645–1647
Gallacher R, Keir D, Harmon N, Stuart G, Leroy S, Hammond JOS et al (2016) The initiation of segmented buoyancy-driven melting during continental breakup. Nat Commun 7:13110. https://doi.org/10.1038/ncomms13110
Geirsson H, Arnadottir T, Volksen C, Jiang W, Sturkell E, Villemin T et al (2006) Current plate movements across the Mid-Atlantic Ridge determined from 5 years of continuous GPS measurements in Iceland. J Geophys Res 111:B09407. https://doi.org/10.1029/2005JB003717
Giusti M, Perrot J, Dziak RP, Sukhovic A, Maia M (2018) The August 2010 earthquake swarm at North FAMOUS–FAMOUS segments, Mid-Atlantic Ridge: geophysical evidence of dike intrusion. Geophys J Int 215:181–195
Grandin R, Socquet A, Binet R, Klinger R, Jacques E, de Chabalier JB et al (2009) September 2005 Manda Hararo-Dabbahu rifting event, Afar (Ethiopia): Constraints provided by geodetic data. J Geophys Res 114: B08404, https://doi.org/10.1029/2008JB005843
Grant JV, Kattenhorn SA (2004) Evolution of vertical faults at an extensional plate boundary, Southwest Iceland. J Struct Geol 26:537–557
Greenfield T, Keir D, Kendall J-M, Ayele A (2019) Low-frequency earthquakes beneath Tullu Moye volcano, Ethiopia, reveal fluid pulses from shallow magma chamber. Earth Planet Sci Lett 526:115782
Grevemeyer I, Hayman NW, Peirce C, Schwardt M, Van Avendonk HJA, Dannowski A et al (2018) Episodic magmatism and serpentinized mantle exhumation at an ultraslow-spreading centre. Nat Geosci 11:444–448
Gu YJ, Lerner-Lam AL, Dziewonski AM, Ekstrom G (2005) Deep structure and seismic anisotropy beneath the East Pacific Rise. Earth Planet Sci Lett 232:259–272
Gudmundsson A (1986) Formation of crustal magma chambers in Iceland. Geology 14:164–166
Gudmundsson A, Backstrom K (1991) Structure and development of the Sveinagja Graben, northeast Iceland. Tectonophysics 200:111–125
Gudmundsson A (1992) Formation and growth of normal faults at the divergent plate boundary in Iceland. Terra Nova 4:464–471
Gudmundsson A (1995) Infrastructure and mechanics of volcanic systems in Iceland. J Volcanol Geoth Res 64:1–22
Hammond JOS, Kendall J-M, Stuart GW, Ebinger CJ, Bastow ID, Keir D et al (2013) Mantle upwelling and initiation of rift segmentation beneath the Afar Depression. Geology 41:635–638
Hartley ME, Thordarson T (2012) Formation of Öskjuvatn caldera at Askja, North Iceland: mechanism of caldera collapse and implications for the lateral flow hypothesis. J Volcanol Geoth Res 227–228:85–101
Hayward NJ, Ebinger CJ (1996) Variation in the along-axis segmentation of the Afar Rift system. Tectonics 15:244–257
Helgason J, Zentilli M (1985) Field characteristics of laterally emplaced dikes: anatomy of an exhumed Miocene dike swarm in Reydarfjordur, Eastern Iceland. Tectonophysics 115:247–274
Hofmann C, Courtillot V, Feraud G, Rochette P, Yirgu G, Ketefo E et al (1997) Timing of the Ethiopian flood basalt event and implications for plume birth and global change. Nature 389:838–841
Hollingsworth J, Leprince S, Ayoub F, Avouac J-P (2013) New constraints on dike injection and fault slip during the 1975–1984 Krafla rift crisis, NE Iceland. J Geophys Res 118:3707–3727

Horst AJ, Varga RJ, Gee JS, Karson JA (2014) Diverse magma flow directions during construction of sheeted dike complexes at fast-to superfast-spreading centers. Earth Planet Sci Lett 408:119–131

Hreinsdottir S, Einarsson P, Sigmundsson F (2001) Crustal deformation at the oblique spreading Reykjanes Peninsula, SW Iceland: GPS measurements from 1993 to 1998. J Geophys Res 106:13803–13816

Husson L, Yamato P, Bezos A (2015) Ultraslow, slow, or fast spreading ridges: arm wrestling between mantle convection and far-field tectonics. Earth Planet Sci Lett 429:205–215

Hutchison W, Mather TA, Pyle DM, Boyce AJ, Gleeson MLM, Yirgu G et al (2018) The evolution of magma during continental rifting: New constraints from the isotopic and trace element signatures of silicic magmas from Ethiopian volcanoes. Earth Planet Sci Lett 489:203–218

Jacques E, Ruegg JC, Lepine JC, Tapponnier P, King GCP, Omar A (1999) Relocation of M $\geq$ 2 events of the 1989 Dobi seismic sequence in Afar: evidence for earthquake migration. Geophys J Int 138:447–469

Jenkins J, Maclennan J, Green RG, Cottaar S, Deuss AF, White RS (2018) Crustal formation on a spreading ridge above a mantle plume: receiver function imaging of the Icelandic crust. J Geophys Res 123:5190–5208

Jian H, Singh SC, Chen YJ, Li J (2017) Evidence of an axial magma chamber beneath the ultraslow spreading Southwest Indian Ridge. Geology 45:143–146

Jokat W, Ritzmann O, Schmidt-Aursch MC, Drachev S, Gauger S, Snow J (2003) Geophysical evidence for reduced melt production on the Arctic ultraslow Gakkel mid-ocean ridge. Nature 423:962–965

Jónsson S, Xu W (2015) Volcanic eruptions in the southern Red Sea during 2007–2013. In: Rasul NMA, Stewart ICF (eds) The Red Sea: the formation, morphology, oceanography and environment of a young ocean basin. Springer Earth System Sciences Heidelberg, pp 175–186

Keiding M, Lund B, Arnadottir T (2009) Earthquakes, stress and strain along an obliquely divergent plate boundary: Reykjanes Peninsula, southwest Iceland. J Geophys Res 114:B09306. https://doi.org/10.1029/2008JB006253

Keir D, Ebinger CJ, Stuart GW, Daly E, Ayele A (2006) Strain accommodation by magmatism and faulting as rifting proceeds to breakup: seismicity of the northern Ethiopian Rift. J Geophys Res 111:B05314. https://doi.org/10.1029/2005JB003748

Keir D, Belachew M, Ebinger CJ, Kendall JM, Hammond JOS, Stuart GW et al (2011) Mapping the evolving strain field during continental breakup from crustal anisotropy in the Afar depression. Nat Commun 2:1–7

Keir D, Bastow ID, Corti G, Mazzarini F, Rooney TO (2015) The origin of along-rift variations in faulting and magmatism in the Ethiopian Rift. Tectonics 34:464–477

Kendall JM, Stuart GW, Ebinger CJ, Bastow ID, Keir D (2005) Magma-assisted rifting in Ethiopia. Nature 433:146–214

Kent GM, Singh SC, Harding AJ, Sinha MC, Orcutt JA, Barton PJ et al (2000) Evidence from three-dimensional seismic reflectivity images for enhanced melt supply beneath mid-ocean ridge discontinuities. Nature 406:614–618

Keranen K, Klemperer SL, Gloaguen R, Eagle Working Group (2004) Three-dimensional seismic imaging of a protoridge axis in the Main Ethiopian Rift. Geology 32:949–952

Kogan L, Fisseha S, Bendick R, Reilinger R, McClusky S, King R (2012) Lithospheric strength and strain localization in continental extension from observations of the East African Rift. J Geophys Res 117:B03402. https://doi.org/10.1029/2011JB008516

Lagabrielle I, Cormier MH (1999) Formation of large summit troughs along the East Pacific Rise as collapse calderas: an evolutionary model. J Geophys Res 104:12971–12988

Lahitte P, Gillot PY, Courtillot V (2003) Silicic central volcanoes as precursors to rift propagation: the Afar case. Earth Planet Sci Lett 207:103–116

Ligi M, Bonatti E, Caratori M, Tontini F, Cipriani A, Cocchi L et al (2011) Initial burst of oceanic crust accretion in the Red Sea due to edge-driven mantle convection. Geology 39:1019–1022

Ligi M, Bonatti E, Bosworth W, Ronca S (2019) Oceanization starts at depth during continental rupturing in the Northern Red Sea. In: Rasul NMA, Stewart ICF (eds) Geological setting, palaeoenvironment and archaeology of the Red Sea. Springer Nature, Switzerland, pp 131–157

Maccaferri F, Rivalta E, Keir D, Acocella A (2014) Off-rift volcanism in rift zones determined by crustal unloading. Nat Geosci 7:297–300

Maccaferri F, Acocella V, Rivalta E (2015) How the differential load induced by normal fault scarps controls the distribution of monogenic volcanism. Geophys Res Lett 42. https://doi.org/10.1002/2015GL065638

Macdonald KC, Fox PJ (1988) The axial summit graben and cross-sectional shape of the East Pacific Rise as indicators of axial magma chambers and recent volcanic eruptions. Earth Planet Sci Lett 88:119–131

Macdonald K, Scheirer D, Carbotte S (1991) Mid-ocean ridges: discontinuities, segments and giant cracks. Science 253:986–994

Macdonald K (1998) Linkages between faulting, volcanism, hydrothermal activity and segmentation on fast spreading centres. In: Buck WR, Delaney PT, Karson JA, Lagabrielle YU (eds) Faulting and magmatism at mid-ocean ridges. AGU Monograph Washington, pp 27–58

Mackenzie GD, Thybo H, Maguire PKH (2005) Crustal velocity structure across the Main Ethiopian Rift: results from two-dimensional wide-angle seismic modelling. Geophys J Int 162:994–1006

Manighetti I, Tapponnier P, Courtillot V, Gallet Y, Jacques E, Gillot PY (2001) Strain transfer between disconnected, propagating rifts in Afar. J Geophys Res 106:13613–13665

Marjanovic M, Carbotte SM, Carton H, Nedimovic NR, Mutter JC, Canales JP (2014) A multi-sill magma plumbing system beneath the axis of the East Pacific Rise. Nat Geosci 7:825–829

Marjanović M, Carbotte SM, Carton HD, Nedimović MR, Canales JP, Mutter JC (2018) Crustal magmatic system beneath the East Pacific Rise (8°20' to 10° 10'N): implications for tectonomagmatic segmentation and crustal melt transport at fast-spreading ridges. Geochem Geophys Geosyst 19:4584–4611

Mark HF, Behn MD, Olive JA, Liu Y (2018) Controls on mid-ocean ridge normal fault seismicity across spreading rates from rate-and-state friction models. J Geophys Res 123:6719–6733

McClusky S, Reilinger R, Ogubazghi G, Amleson A, Healeb B, Vernant P et al (2010) Kinematics of the southern Red Sea-Afar triple junction and implications for plate dynamics. Geophys Res Lett 37:L05301. https://doi.org/10.1029/2009GL041127

Medynski S, Pik R, Burnard P, Dumont S, Grandin R, Williams A et al (2016) Magmatic cycles pace tectonic and morphological expression of rifting (Afar depression, Ethiopia). Earth Planet Sci Lett 446:77–88

Michael PJ, Langmuir CH, Dick HJB, Snow JE, Goldstein SL, Graham DW et al (2003) Magmatic and amagmatic seafloor generation at the ultraslow-spreading Gakkel ridge, Arctic Ocean. Nature 425:956–961

Mitchell NC, Park Y (2014) Nature of crust in the central Red Sea. Tectonophysics 628:123–139

Mitchell NC, Stewart ICF (2018) The modest seismicity of the northern Red Sea rift. Geophys J Int 214:1507–1523

Mohr P (1967) Major volcano-tectonic lineament in the Ethiopian rift system. Nature 213:664–665

Mohr PA, Wood CA (1976) Volcano spacing and lithospheric attenuation in the Eastern Rift of Africa. Earth Planet Sci Lett 33:126–144

Mohr P (1983) Ethiopian flood basalt province. Nature 303:577–584

Montesi LGJ, Behn MD (2007) Mantle flow and melting underneath oblique and ultraslow mid-ocean Ridges. Geophys Res Lett 34:L24307. https://doi.org/10.1029/2007GL031067

Mutch JF, Maclennan J, Shorttle O, Edmonds M, Rudge JF (2019) Rapid transcrustal magma movement under Iceland. Nat Geosci 12(569):573

Mutter JC, Karson JA (1992) Structural processes at slow-spreading ridges. Science 257:627–634

Njinju EA, Kolawole F, Atekwana EA, Stamps DS, Atekwana EA, Abdelsalam MG et al (2019) Terrestrial heat flow in the Malawi Rifted Zone, East Africa: implications for tectono-thermal inheritance in continental rift basins. J Volcanol Geoth Res 387:106656

Niu Y, Hekinian R (1997) Spreading rate dependence of the extent of mantle melting beneath ocean ridges. Nature 385:326–329

Nobile A, Pagli C, Keir D, Wright TJ, Ayele A, Ruch J et al (2012) Dyke-fault interaction during the 2004 Dallol intrusion at the northern edge of the Erta Ale Ridge (Afar, Ethiopia). Geophys Res Lett 39:L19305. https://doi.org/10.1029/2012GL053152

Nooner SL, Webb SC, Buck WR, Cormier M-H (2014) Post eruption inflation of the East Pacific Rise at 9°50' N. Geochem Geophys Geosyst 15:2676–2688

O'Connor JM, Jokat W, Regelous M, Kuiper KF, Miggins DP, Koppers AAP (2019) Superplume mantle tracked isotopically the length of Africa from the Indian Ocean to the Red Sea. Nat Commun 10:5493. https://doi.org/10.1038/s41467-019-13181-7

Omar GI, Steckler MS (1995) Fission track evidence on the initial rifting of the Red Sea: two pulses, no propagation. Science 270:1341–1344

Pagli C, Wright TJ, Ebinger CJ, Yun SH, Cann JR, Barnie T et al (2012) Shallow axial magma chamber at the slow spreading Erta Ale Ridge. Nat Geosci. https://doi.org/10.1038/NGEO1414

Pagli C, Wang H, Wright TJ, Calais E, Lewi E (2014) Current plate boundary deformation of the Afar rift from a 3-D velocity field inversion of InSAR and GPS. J Geophys Res 119:8562–8575

Pagli C, Yun S-H, Ebinger C, Keir D, Wang H (2019) Strike-slip tectonics during rift linkage. Geology 47:31–34

Pallister JS, McCausland WA, Jonsson S, Lu Z, Zahran HM, El Hadidy S et al (2010) Broad accommodation of rift-related extension recorder by dyke intrusion in Saudi Arabia. Nat Geosci 3:708–712

Park Y, Nyblade AA (2006) P-wave tomography reveals a westward dipping low velocity zone beneath the Kenya Rift. Geophys Res Lett 33:L07311. https://doi.org/10.1029/2005GL025605

Parnell-Turner RE, Mittelstaedt E, Kurz MD, Jones MR, Soule SA, Klein F et al (2018) The final stages of slip and volcanism on an oceanic detachment fault at 13° 48'N, Mid-Atlantic Ridge. Geochem Geophys Geosyst 19:3115–3127

Passarelli L, Rivalta E, Shuler A (2014) Dike intrusions during rifting episodes obey scaling relationships similar to earthquakes. Sci Rep 4:3886. https://doi.org/10.1038/srep03886

Peccerillo A, Donati C, Santo AP, Orlando A, Yirgu G, Ayalew D (2007) Petrogenesis of silicic peralkaline rocks in the Ethiopian rift: geochemical evidence and volcanological implications. J Afr Earth Sci 48:161–173

Peirce C, Sinha MC (2008) Life and death of axial volcanic ridges: segmentation and crustal accretion at the Reykjanes Ridge. Earth Planet Sci Lett 274:112–120

Perez-Gussinyé M, Metois M, Fernandez M, Verges J, Fullea J, Lowry A (2009) Effective elastic thickness of Africa and its relationship to other proxies for lithospheric structure and surface tectonics. Earth Planet Sci Lett 287:152–167

Perfit MR, Chadwick WW (1998) Magmatism at mid-ocean ridges: constraints from volcanological and geochemical investigations. In: Buck WR, Delaney PT, Karson JA, Lagabrielle Y (eds) Faulting and magmatism at mid-ocean ridges. AGU Geophysical Monograph Series Washington, vol 106, pp 59–115

Perlt J, Heinert M, Niemeier W (2008) The continental margin in Iceland—a snapshot derived from combined GPS networks. Tectonophysics 447:155–166

Pinzuti P, Mignan A, King GCP (2010) Surface morphology of active normal faults in hard rock: implications for the mechanics of the Asal Rift, Djibouti. Earth Planet Sci Lett 299:169–179

Pollard DD, Aydin A (1984) Propagation and linkage of oceanic ridge segments. J Geophys Res 89:10017–10028

Purdy GM, Kong LSL, Christenson GL, Solomon SC (1991) Relationship between spreading rate and the seismic structure of mid-ocean ridges. Nature 355:815–817

Reiss MC, Muirhead JD, Laizer AS, Link F, Kazimoto EO, Ebinger CJ et al (2021) The impact of complex volcanic plumbing on the nature of seismicity in the developing magmatic natron rift, Tanzania. Front Earth Sci 8:609805, https://doi.org/10.3389/feart.2020.609805

Reston T (2018) Flipping detachments: the kinematics of ultraslow spreading ridges. Earth Planet Sci Lett 503:144–157

Rooney TO (2020a) The Cenozoic magmatism of East-Africa: Part I—flood basalts and pulsed magmatism. Lithos 286–287:264–301

Rooney TO (2020b) The cenozoic magmatism of East Africa: Part II—rifting of the mobile belt. Lithos 360–361:105291

Rowland JV, Baker E, Ebinger CJ, Keir D, Kidane T, Biggs J et al (2007) Fault growth at a nascent slow-spreading ridge: the 2005 Dabbahu rifting episode, Afar. Geophys J Int 171:1226–1246

Rowley DB, Forte AM, Rowan CJ, Glišović P, Moucha R, Grand SP (2016) Kinematics and dynamics of the East Pacific Rise linked to a stable, deep mantle upwelling. Sci Adv 2:e1601107

Saemundsson K, Sigugeirsson MA, Fridleifsson GO (2020) Geology and structure of the Reykjanes volcanic system, Iceland. J Volcanol Geoth Res 391:106501

Sandwell DT, Smith WHF (2009) Global marine gravity from retracked Geosat and ERS-1 altimetry: ridge segmentation versus spreading rate. J Geophys Res 114:B01411. https://doi.org/10.1029/2008JB006008

Schettino A, Macchiavelli C, Pierantoni PP, Zanoni D, Rasul N (2016) Recent kinematics of the tectonic plates surrounding the Red Sea and Gulf of Aden. Geophys J Int 207:457–480

Schlindwein V, Schmid F (2016) Mid-ocean-ridge seismicity reveals extreme types of ocean lithosphere. Nature 535:276–279

Searle RC, Keeton JA, Owens RB, White RS, Mecklenburgh R, Parsons B et al (1998) The Reykjanes ridge: structure and tectonics of a hot-spot influenced slow spreading ridge, from multibeam bathymetry, gravity and magnetic investigations. Earth Planet Sci Lett 160:463–478

Searle RC, Murton BJ, Achenbach K, LeBas T, Tivey M, Yeo I et al (2010) Structure and development of an axial volcanic ridge: Mid-Atlantic Ridge, 45°N. Earth Planet Sci Lett 299:228–241

Shah AK, Buck WR (2003) Plate bending stresses at axial highs, and implications for faulting behaviour. Earth Planet Sci Lett 211:343–356

Sibrant ALR, Mittelstaedt E, Davaille A, Pauchard L, Aubertin A, Auffray L et al (2018) Accretion mode of oceanic ridges governed by axial mechanical strength. Nat Geosci 11:274–279

Sigmundsson F (1992) Tectonic implications of the 1989 Afar earthquake sequence. Geophys Res Lett 19:877–880

Sigmundsson F, Vadon H, Massonnet D (1997) Readjustment of the Krafla spreading segment to crustal rifting measured by satellite radar interferometry. Geophys Res Lett 24:1843–1846

Sigmundsson F (2006a) Magma does the splits. Nature 442:251–252

Sigmundsson F (2006b) Iceland geodynamics: crustal deformation and divergent plate tectonics. Springer, Berlin, 209 pp

Sigmundsson F, Hooper A, Hreinsdottir S, Vogfjord KS, Ofeigsson DG, Heimisson et al (2015) Segmented lateral dyke growth in a rifting event at Barðarbunga volcanic system, Iceland. Nature 517:191–195

Sigmundsson F, Einarsson P, Hjartardottir AR, Drouin V, Jonsdottir K, Arnadottir T et al (2020) Geodynamics of Iceland and the signatures of plate spreading. J Volcanol Geoth Res 391:106436

Sigurdsson O (1980) Surface deformation of the Krafla fissure swarm in two rifting events. J Geophys Res 47:154–159

Singh SC, Crawford WC, Carton H, Seher T, Combier V, Cannat M (2006) Discovery of a magma chamber and faults beneath a Mid-Atlantic Ridge hydrothermal field. Nature 442:1029–1032

Sinton J, Gronvole K, Saemundsson K (2005) Postglacial eruptive history of the Western Volcanic Zone, Iceland. Geochem Geophys Geosyst 6:Q12009. https://doi.org/10.1029/2005GC001021

Smittarello D, Grandin R, De Chabalier J-B, Doubre C, Deprez A, Masson F et al (2016) Transient deformation in the Asal-Ghoubbet Rift (Djibouti) since the 1978 diking event: is deformation controlled by magma supply rates? J Geophys Res 121:6030–6052

Snow JE, Edmonds HN (2007) Ultraslow-spreading ridges rapid paradigm changes. Oceanography 20:90–101

Soule SA, Escartin J, Fornari DJ (2009) A record of eruption and intrusion at a fast spreading ridge axis: axial summit trough of the East pacific Rise at 9–10°N. Geochem Geophys Geosyst 10:Q10T07. https://doi.org/10.1029/2008GC002354

Stamps DS, Saria E, Kreemer C (2018) A geodetic strain rate model for the east african rift system. Sci Rep 8:732. https://doi.org/10.1038/s41598-017-19097-w

Standish JJ, Sims KWW (2010) Young off-axis volcanism along the ultraslow-spreading Southwest Indian Ridge. Nat Geosci 3:286–292

Sturkell E, Sigmundsson F (2000) Continuous deflation of the Askja caldera, Iceland, during the 1983–1998 noneruptive period. J Geophys Res 105:25671–25684

Takada A (1994) The influence of regional stress and magmatic input on styles of monogenetic and polygenetic volcanism. J Geophys Res 99:13563–13573

Tan YJ, Tolstoy M, Waldhauser F, Wilcox WSD (2016) Dynamics of a seafloor-spreading episode at the East Pacific Rise. Nature 540:261–265

Tapponnier P, Armijo R, Manighetti I, Courtillot V (1990) Bookshelf faulting and horizontal block rotations between overlapping rifts in Southern Afar. Geophys Res Lett 17:1–4

Tarantola A, Ruegg JC, Lepine JC (1979) Geodetic evidence for rifting in Afar. A brittle-elastic model of the behavior of the lithosphere. Earth Planet Sci Lett 45:435–444

Thordarson T, Self S (1993) The Laki (Skaftar Fires) and Grimsvotn eruptions in 1783–1785. Bull Volcanol 55:233–263

Thordarson T, Larsen G (2007) Volcanism in historical time: volcano types, eruptions styles and eruptive history. J Geodyn 43:118–152

Tolstoy M, Cowen JP, Baker ET, Fornari DJ, Rubin KH, Shank TM et al (2006) A sea-floor spreading event captured by seismometers. Science 314:1920–1922

Tolstoy M, Waldhauser F, Bohnenstiehl DR, Weekly RT, Kim WY (2008) Seismic identification of along-axis hydrothermal flow on the East Pacific Rise. Nature 451:181–195

Toomey DR, Hooft EEE (2008) Mantle upwelling, magmatic differentiation, and the meaning of axial depth at fast-spreading ridges. Geology 36:679–682

Trippanera D, Ruch J, Passone L, Jónsson S (2019) Structural mapping of dike-induced faulting in Harrat Lunayyir (Saudi Arabia) by using high resolution drone imagery. Front Earth Sci 7:168. https://doi.org/10.3389/feart.2019.00168

Tryggvason E (1984) Widening of the Krafla fissure swarm during the 1975–1981 volcano-tectonic episode. Bull Volcanol 47:47–69

Tucholke BE, Behn MD, Buck RW, Lin J (2008) Role of melt supply in oceanic detachment faulting and formation of megamullions. Geology 36:455–458

Upcott NM, Mukasa RK, Ebinger CJ, Karner GD (1996) Along-axis segmentation and isostasy in the Western rift, East Africa. J Geophys Res 101:3247–3268

Vanderbeek BP, Toomey DR, Hooft EEE, Wilcock WSD (2016) Segmentation of mid-ocean ridges attributed to oblique mantle divergence. Nat Geosci 9:636–642

Varet J (2018) Geology of Afar (East Africa). Springer International Publishing AG, 345 pp

Vigny C, de Chabalier JB, Ruegg JC, Huchon P, Feigl KL, Cattin et al (2007) Twenty-five years of geodetic measurements along the Tadjoura-Asal rift system, Djibuti, East Africa. J Geophys Res 112: B06410. https://doi.org/10.1029/2004JB003230

Wadge G, Biggs J, Lloyd R, Kendall J-M (2016) Historical volcanism and the state of stress in the East African Rift system. Front Earth Sci 4:86. https://doi.org/10.3389/feart.2016.00086

Waters CL, Sims KWW, Klein EM, White SM, Reagan MK, Girard G (2013) Sill to surface: linking young off-axis volcanism with subsurface melt at the overlapping spreading center at 9°03′N East Pacific Rise. Earth Planet Sci Lett 369–370:59–70

Wernicke B (1985) Uniform-sense normal simple shear of the continental lithosphere. Can J Earth Sci 22:108–125

White SM, Haymon RM, Fornari DJ, Perfit MR, MacDonald KC (2002) Correlation between volcanic and tectonic segmentation of fast-spreading ridges: evidence from volcanic structures and lava flow morphology on the East Pacific Rise at 9°-10°N. J Geophys Res 107:2173. https://doi.org/10.1029/2001JB000571

Williams FM, Williams MAJ, Aumento F (2004) Tensional fissures and crustal extension rates in the northern part of the Main Ethiopian Rift. J Afr Earth Sci 38:183–197

Wilson DJ, Robinson AH, Hobbs RW, Peirce C, Funnell MJ (2019) Does intermediate spreading-rate oceanic crust result from episodic transition between magmatic and magma-dominated, faulting-enhanced spreading? The Costa Rica Rift example. Geophys J Int 218:1617–1641

Wright TJ, Ebinger C, Biggs J, Ayele A, Yirgu G, Keir D et al (2006) Magma maintained rift segmentation at continental rupture in the 2005 Afar dyking episode. Nature 442:291–294

Wright TJ, Sigmundsson F, Pagli C, Belachew M, Hamling IJ, Brandsdottir B et al (2012) Geophysical constraints on the dynamics of spreading centres from rifting episodes on land. Nat Geosci 5:242–250

Xu M, Canales JP, Carbotte SM, Carton H, Nedimovic MR, Mutter JC (2014) Variations in axial magma lens properties along the East Pacific Rise (9°30′N–10°00′N) from swath 3-D seismic imaging and 1-D waveform inversion. J Geophys Res 119:2721–2744

Xu W, Ruch J, Jonsson S (2015) Birth of two volcanic islands in the southern Red Sea. Nat Commun 6:7104. https://doi.org/10.1038/ncomms8104

Xu W, Rivalta E, Li X (2017) Magmatic architecture within a rift segment: Articulate axial magma storage at Erta Ale volcano, Ethiopia. Earth Planet Sci Lett 476:79–86